ORIGINAL ARTICLE

Comparative genomic and transcriptomic analyses reveal distinct response strategies to hypoxia by *Vibrio parahaemolyticus* isolates of clinical and aquatic animal origins

Huihui Xu[1], Beiyu Zhang[1], Pan Yu[1], Meng Sun[1], Lu Xie[2*] and Lanming Chen[1*]

Abstract

Purpose *Vibrio parahaemolyticus* is a leading seafood borne pathogen worldwide. The aim of this study was to decipher the response mechanism of *V. parahaemolyticus* isolates of clinical and aquatic animal origins to the hypoxic condition, which challenges the bacterial survival in the host and in the environment.

Methods Growth profiles of *V. parahaemolyticus* isolates ($n = 5$) of clinical and aquatic animal origins were examined at different stress conditions (osmolality, acid, temperature, and O_2 concentrations). Draft genomes of the *V. parahaemolyticus* isolates were determined using the Illumina sequencing technique. Comparative genomic analysis were performed to identify and validate the hypoxic tolerance-related genes.

Results The *V. parahaemolyticus* isolates had an oxygen concentration-dependent growth mode, and the 10% O_2 condition strongly inhibited the bacterial growth, when incubated in TSB medium (pH 8.5, 3% NaCl) at 37 °C. Unexpectedly, in marked contrast to the normal 21% O_2 condition, the 10% O_2 treatment for 24 h significantly increased biofilm formation of *V. parahaemolyticus* isolates ($p < 0.05$). Draft genome sequences of four *V. parahaemolyticus* isolates of aquatic animal origins were determined (4.914–5.3530 Mb), which carried mobile genetic elements ($n = 12$–29). Genome-wide gene expression changes triggered by the hypoxic condition were further examined. Comparative transcriptomic analyses unveiled multiple molecular strategies employed by the bacterium to mitigate the cell damage caused by the hypoxia. Of note, the pathogenic *V. parahaemolyticus* ATCC17802 down-regulated and/or shut down ten metabolic pathways to reduce cell viability and maintain cell structure under the hypoxic stress.

Conclusions The results of this study fill prior gaps in the response mechanism of *V. parahaemolyticus* to the hypoxic condition. Different tolerance to hypoxia contributes to the persistence of pathogenic *V. parahaemolyticus* in the niches.

Keywords *Vibrio parahaemolyticus*, Hypoxia, Genome, Transcriptome, Foodborne pathogen

*Correspondence:
Lu Xie
luxiex2017@outlook.com
Lanming Chen
lmchen@shou.edu.cn
Full list of author information is available at the end of the article

Xu *et al. Annals of Microbiology*   (2024) 74:20

Page 2 of 23

Introduction

Vibrio parahaemolyticus is a Gram-negative bacterium that inhabits in marine and estuarine environments worldwide (Li et al. 2019). Consuming raw seafood, incomplete food processing, or cross-contamination during food processing can lead to *V. parahaemolyticus* infection in humans. The clinical manifestations are gastroenteritis, organ infection, septicaemia, and even death (Li et al. 2019). In the United States, more than 50% of foodborne gastrointestinal-Vibriosis cases are caused by *V. parahaemolyticus* (Karan et al. 2021), which leads to about 80,000 illnesses each year (https://www.cdc.gov/Vibrio/, accessed on November 1, 2022). In China, a national surveillance of 152,792 patients of all ages with acute diarrhea in 31 provinces was administered in 2009–2018. *V. parahaemolyticus* was found to be the third common bacterial pathogen and contributed to 10.83% of all positive detection (Wang et al. 2021). The pathogenicity of *V. parahaemolyticus* is strongly associated with the expression of thermostable direct hemolysin (TDH) and/or TDH-related hemolysin (TRH) (Pazhani et al. 2021).

V. parahaemolyticus is frequently detected in seafood (Vu et al. 2022). The elevated seawater temperatures caused by rising global temperatures from climate change may affect transmission of waterborne pathogenic bacteria (Murray et al. 2020; Tong et al. 2022). For instance, the number of days per year suitable for Vibrio in the Baltic Sea and along the north east coast of the United States reached 107 in 2018, double the early 1980s baseline (Murray et al. 2020). As the sea temperature rises, oxygen (O_2) becomes less soluble via a process known as deoxygenation (Gao et al. 2012). Low oxygen condition refers to oxygen partial pressure of 0–10% (Chen et al. 2007). Compared to strictly aerobic or strictly anaerobic conditions, the hypoxic zone has unique biological properties in the environment (Pohl et al. 2022).

The respiration of oxygen is the main source of energy for biological cells (Bueno et al. 2020). The low oxygen condition impacts on cellular enzymatic activity, such as dehydrogenase and superoxide dismutase (Obbard et al. 1994; Reaney et al. 2005), and also change how quickly organisms metabolize and respire (Oschlies et al. 2018). Studies have indicated that waterborne pathogen *Vibrio cholerae* can exchange common oxygen respiratory terminal oxidases with high-oxygen-affinity terminal oxidases (H–O-ATOs), using the fermentation pathway, with some electron acceptors (EAs) such as fumarate, and nitrate (Bueno et al. 2018; Heidelberg et al. 2000). It has also been reported that biofilm formation of common pathogens *Pseudomonas aeruginosa*, *Streptococcus aureus*, and *Escherichia coli* induces the production of hypoxia-related enzymes such as H–O-ATOs, nitrate reductases, and anaerobic ribonucleotide reductases (Crespo et al. 2016; Jo et al. 2017; Létoffé et al. 2017). Biofilm, constructed primarily by autogenic extracellular polymeric substances, can protect bacteria from the environmental stress, hinder phagocytosis, and thus confer the capacity for long-term colonization and persistence in the host (Thi et al. 2020). The enteric pathogen *V. parahaemolyticus* can access, colonize, and proliferate within the human intestine with low oxygen level, causing severe diarrhea disease (Bueno et al. 2020; Sun et al. 2022). Nevertheless, to the best of our knowledge, how *V. parahaemolyticus* responses to the low oxygen condition has not yet been unveiled so far.

In our previous studies, a number of *V. parahaemolyticus* isolates of aquatic animal origins were isolated, identified and characterized (Su and Chen 2020; Sun et al. 2014; Xu et al. 2022a; Xu et al. 2022b; Yang et al. 2020; Yu et al. 2022; Zhu et al. 2020). Based on these studies, in the present study, we deciphered for the first time the fitness mechanism of *V. parahaemolyticus* of aquatic animal and human clinical origins under the hypoxic condition. The major objectives of this study were (1) to investigate growth features of *V. parahaemolyticus* isolates ($n=5$) at different concentrations of oxygen (21–5% O_2); (2) to monitor dynamic process of biofilm formation, and observe morphological cell structure changes of the *V. parahaemolyticus* isolates at the hypoxic condition (e.g., 10% O_2); and (3) to decipher the molecular mechanism of *V. parahaemolyticus* response to the hypoxic condition by comparative genomics and transcriptomics analyses. The results of this study provide the first experimental evidence for multiple molecular strategies developed by *V. parahaemolyticus* to deal with the hypoxia.

Materials and methods

V. parahaemolyticus strains and culture conditions

The *V. parahaemolyticus* B8-26, B1-21, N2-5, and L7-40 strains (Table 1) were individually inoculated (1%, v/v) into 5-mL Tryptone Soya Broth (TSB) (Beijing Land Bridge Technology, Beijing, China), and routinely incubated aerobically with shaking at 180 r/min at 37 °C incubator (Shanghai Zhichu Instrument, Shanghai, China). *V. parahaemolyticus* ATCC17802 was used as a positive control strain, which was first isolated in 1950, leading to the outbreak of human acute gastroenteritis in Japan (Fujino et al. 1953). The overnight cultures were re-inoculated in fresh TSB, incubated to middle logarithmic growth phase (mid-LGP), and used in the following assays.

Antibiotic resistance and heavy metal tolerance assays

The *V. parahaemolyticus* isolates was tested for antibiotic susceptibility using the standard disc diffusion method of Clinical and Laboratory Standards Institute (CLSI,

Table 1 The phenotype features of the *V. parahaemolyticus* isolates used in this study

Strain	Origin	Toxin gene		Resistance phenotype		
		tdh	*trh*	Heavy metal	Antimicrobial agent	Source
B8-26	Shellfish (*Solen strictus*)	-	-	$Cu^{2+}/Hg^{2+}/Cd^{2+}/Zn^{2+}$	AMP/KAN/RIF/STR	This study
B1-21	Shellfish (*Corbicula aurea*)	-	-	$Hg^{2+}/Zn^{2+}/Ni^{2+}/Pb^{2+}$	AMP/KAN/RIF/STR	This study
N2-5	Shrimp (*Oratosquilla oratoria*)	-	-	Hg^{2+}/Cd^{2+}	AMP/KAN/RIF/STR/TET	This study
L7-40	Fish (*Ctenopharyngodon idellu*)	-	-	$Hg^{2+}/Cd^{2+}/Cr^{2+}/Zn^{2+}$	AMP/KAN/RIF/STR	This study
ATCC17802	Shirasu-food	-	+	Hg^{2+}/Zn^{2+}	AMP	Fujino et al. 1953

-: unavailable

M100-S28, 2018), USA. The Mueller–Hinton (MH) medium and ten antibiotic discs were purchased from OXOID, Basingstoke, UK. *Escherichia coli* ATCC25922 was used as a quality control strain (Su and Chen 2020).

Tolerance of the *V. parahaemolyticus* isolates to heavy metals was examined using the standard broth dilution testing (microdilution) (Su and Chen 2020; Xu et al. 2022a; Yu et al. 2022). Eight heavy metals (Analytical Reagents) were purchased from Sinopharm Chemical Reagent Co., Ltd., Shanghai, China. *E. coli* K12 was used as a quality control strain (Su and Chen 2020).

Growth curve assay of the *V. parahaemolyticus* isolates at different NaCl concentrations, pH and temperatures

The TSB medium was individually adjusted to different NaCl concentrations (0.5%, 1%, 2%, 3%, 4%, and 5%) and pH values (6.0, 6.5, 7.0, 7.5, 8.0, and 8.5) (Sun et al. 2014). Growth curves of the *V. parahaemolyticus* isolates under the different NaCl (0.5–5%), and pH (6.0–8.5) conditions were individually measured at 37 °C for 40 h using Multimode Microplate Reader (BioTek Instruments, USA). The absorbance value at 600 nm (OD_{600}) was used as a parameter for bacterial biomass (Yao et al. 2020). Growth curves of the *V. parahaemolyticus* isolates in the TSB (pH8.5, 3% NaCl) were also measured at 37 °C, and 25 °C for 40 h, respectively.

Growth curve assay of the *V. parahaemolyticus* isolates at different concentrations of O_2

Growth curves of the *V. parahaemolyticus* isolates at different concentrations of O_2 were measured as described previously (Tian et al. 2020) with minor modifications. Briefly, the *V. parahaemolyticus* isolates were individually inoculated in the 5-mL TSB (pH8.5, 3% NaCl), which was adjusted and equilibrated to different concentrations of O_2 (21%, 18%, 15%, 10%, and 5% O_2) using the nitrogen-blowing instrument (Wen Dong Chemical, Shanghai,

China). The O_2 concentrations were monitored using CY-12C Oxygen Meter (Hangzhou Jiachang Electronic Technology Co., Ltd, Hangzhou, China). Under the different O_2 conditions (21–5% O_2), *V. parahaemolyticus* isolate was individually inoculated into thirty glass culture tubes (15×1.6 cm), which were sealed with sealing film (Beideng Medical Co., Ltd., Jiangsu, China), and incubated with shaking at 180 r/min at 37 °C. Instead of a bioreactor, the simple continuous culture condition allowed to measure OD_{600} values every 4 h for 40 h from three independent tubes using the Multimode Microplate Reader (BioTek Instruments, USA). Meanwhile, O_2 concentrations in air within the tubes were measured correspondingly. Low oxygen condition refers to oxygen partial pressure of 0–10%, which corresponds to a range of dissolved oxygen in water body at room temperature and pressure of 0–4.5 mg/L (Chen et al. 2007).

Biofilm formation assay

Biofilm formation of the *V. parahaemolyticus* isolates was determined using the crystal violet staining method as described in our previous report (Yang et al. 2020). Briefly, 1 mL/well of each *V. parahaemolyticus* culture (adjusted $OD_{600} = 0.4$) was inoculated into 12-well bacterial culture plates (Shanghai Sangon Biological Engineering Technology and Service Co., Ltd., Shanghai, China). The plates were statically incubated at the 21% O_2, and 10% O_2 conditions, respectively. Biofilms formed at 12 h, 24 h, 36 h, 48 h, and 60 h at 37 °C were individually stained, washed, fixed, and measured as described previously (Yang et al. 2020). The 0.1 M phosphate buffer saline (PBS) (pH 7.2–7.4), and 0.25% crystal violet were purchased from the Sangon (Shanghai, China).

Scanning electron microscope (SEM) assay

Preparation of samples for SEM assay was performed according to the method described previously (Yang et al.

Xu *et al. Annals of Microbiology*   (2024) 74:20

Page 4 of 23

2020). Briefly, the *V. parahaemolyticus* isolates were individually incubated in the TSB (3% NaCl, pH 8.5) at the 21% O$_2$, and 10% O$_2$ conditions at 37 °C for 24 h, respectively. Aliquots of 1.5-mL bacterial culture were centrifuged at 8000 g for 5 min at 4 °C, and the cell pellet was wash with 1×PBS (pH 7.2–7.4, Sangon, China), fixed with glutaraldehyde (Bioengineering Co., Ltd., Shanghai, China), and observed using the SU5000 SEM (Hitachi, Tokyo, Japan, 5.0 kV, ×30,000).

Genome sequencing, assembly, and annotation

The *V. parahaemolyticus* isolates were routinely incubated in the TSB (3% NaCl, pH 8.5) at 37 °C to the mid-LGP. The genomic DNA was prepared using TIANamp Bacteria DNA Kit (Tiangen Biochemical Technology Co Ltd., Beijing, China). Three separately produced DNA samples were used for each of the *V. parahaemolyticus* isolates. Only high quality genomic DNA samples (A$_{260}$/$_{280}$ = 1.8–2.0) were subjected to genome sequencing (Xu et al. 2022a).

Whole-genome sequencing was conducted by Shanghai Majorbio Bio-Pharm Technology Co., Ltd. (Shanghai, China) using the Illumina Hiseq×10 (Illumina, San Diego, CA, USA) platform (Xu et al. 2022a). The insert size of PE150 (pair-end) sequencing was 400 bp. Low-quality sequence filtering; high-quality sequence assembly; annotation of coding sequences (CDSs), rRNA genes, and tRNA genes; and prediction of Clusters of Orthologous Groups (COG) of proteins were performed using the same software with default parameters as described in our recent report (Xu et al. 2022a).

The virulence factor database (http://www.mgc.ac.cn/VFs) and antibiotic resistance gene database (http://arpcard.Mcmaster.ca) were used to detect virulence- and antibiotic resistance-related genes in the *V. parahaemolyticus* genomes, respectively. Genomic isolands (GIs), prophages, integrons (INs), insertion sequences (ISs), and clustered regularly interspaced palindromic repeats (CRISPR)-Cas systems were predicted using the same software with default parameters as described in our recent report (Xu et al. 2022a) The MGEs were ordered according to the numbers of the Scaffolds on which they were present (see the corresponding Supplementary Tables).

Phylogenetic tree assay

A total of seventy-eight *V. parahaemolyticus* isolates were subjected for a phylogenetic tree, of which complete genome sequences of seventy-three *V. parahaemolyticus* isolates were downloaded from the GenBank database, together with draft genome sequence of *V. parahaemolyticus* ATCC17802 (Table S1). Amino acid data sets of single-copy orthologs of the *V. parahaemolyticus* genomes,

coupled with the four genomes determined in this study, were analyzed using OrthoFinder (version 2.2.6) software (Emms and Kelly 2019). The phylogenetic tree was constructed using the RAxML (version 8) software (Stamatakis 2014) with 1,000 bootstrap replications and a cut-off threshold of ≥ 50% bootstrap values.

Illumina RNA sequencing and analysis

The *V. parahaemolyticus* isolates were individually incubated in the TSB (3% NaCl, pH 8.5) under the 10% condition at 37 °C for 24 h. Total RNA was extracted using RNeasy Protect Bacteria Mini Kit, QIAGEN RNeasy Mini Kit. The DNA was removed from the extracted RNA samples using RNase-Free DNase Set (QIAGEN Biotech Co. Ltd., Frankfurt, Germany). The Illumina RNA-sequencing was conducted by Shanghai Majorbio Bio-pharm Technology Co. Ltd. (Shanghai, China) using Illumina HiSeq 2500 platform (Illumina, USA). Three separately prepared RNA samples were used for each of the *V. parahaemolyticus* isolates. The *V. parahaemolyticus* isolates grown under the 21% O$_2$ condition were individually used as controls.

Gene expression was analyzed using the RNA-Seq by Expectation–Maximization (RSEM) software (version1.3.3, http://deweylab.github.io/RSEM/). The criteria of fold changes ≥ 2.0 or ≤ 0.5 and *p*-values < 0.05 were used to define differentially expressed genes (DEGs). Gene set enrichment analyses (GSEA) were performed if the enrichment test *p*-values were less than 0.05 (Yang et al. 2020; Yu et al. 2022).

Reverse transcription real time-quantitative PCR (RT-qPCR) assay

Reverse transcription was performed using PrimeScriptTM RT reagent Kit with gDNA Eraser (Perfect Real Time) (QIAGEN Biotech Co. Ltd., Hilden, Germany). The TB Green® Premix Ex Taq™ II (TliRNaseH Plus) (Takara Biomedical Technology Co., Ltd., Beijing, China) was used for relative quantitative PCR with 16 s RNA as the internal reference gene. The RT-qPCR reaction was performed using the Fast Real-Time analyzer (Applied Biosystems, Foster City, California, USA). with the following protocol: 50 °C for 2 min; 95 °C pre-denaturation for 10 min; and 95 °C denaturation for 15 s, 60 °C annealing for 1 min, for 40 cycles. The relative expression levels of target gene and internal reference gene were calculated by $2^{-\Delta\Delta Ct}$ (Yang et al. 2020). The primers targeting the representative DEGs were designed (Table S2), and synthesized by the Sangon (Shanghai, China).

Statistical analysis

The experimental data were analyzed using the SPSS software (version 17.0, SPSS Inc., Chicago, IL, USA).

Differences between the means and changes in the samples were compared by one-way analysis of variance using the least-significant difference (LSD) method, with the level of significance set at $p < 0.05$. All tests were conducted in triplicate.

Results

Phenotypes of the *V. parahaemolyticus* isolates

V. parahaemolyticus B8-26, B1-21, N2-5, and L7-40 strains were used in this study, which were isolated from two species of shellfish (*Solen strictus* and *Corbicula aurea*), one species of crustacean (*Oratosquilla oratoria*), and one species of fish (*Ctenopharyngodon idellus*), respectively, in Shanghai, China in July and August of 2017 (Su and Chen 2020). The resistance of the strains to ten antibiotics were evaluated, and the results indicated that they were all resistant to ampicillin (AMP), kanamycin (KAN), rifampicin (RIF), and streptomycin (STR), while *V. parahaemolyticus* N2-5 was also resistant to tetracycline (TET) (Table 1). Meanwhile, these four isolates had different heavy metal-tolerance profiles (Table 1). For instance, *V. parahaemolyticus* B8-26 was tolerant to $Hg^{2+}/Cd^{2+}/Cu^{2+}/Zn^{2+}$, while *V. parahaemolyticus* B1-21 to $Hg^{2+}/Ni^{2+}/Pb^{2+}/Zn^{2+}$. In addition, *V. parahaemolyticus* ATCC17802 isolate of the human clinical origin was resistant to AMP (Jin et al. 2021), as well as Hg^{2+}/Zn^{2+} (Melo-López et al. 2021).

Growth profiles of the *V. parahaemolyticus* isolates at different salinity concentrations, pH, temperatures, and oxygen concentrations

V. parahaemolyticus is a halophilic bacterium that inhabits in marine and estuarine environments worldwide (Li et al. 2019). We wondered growth features of the *V. parahaemolyticus* isolates of aquatic animal origins. Thus, we determined their growth curves in the TSB (pH 8.5) under the 0.5–5% NaCl conditions at 37 °C. As shown in Fig. S1 (A–E), all the *V. parahaemolyticus* isolates grew poorly at 0.5% NaCl. However, the increased NaCl concentration (1%) significantly promoted the bacterial growth ($p < 0.05$). Although all the isolates grew exuberantly at 2–5% NaCl, the highest biomass was observed when grew at 3% NaCl, showing the maximum OD_{600} values (0.94–1.12) at stationary growth phase (SGP). Exceptionally, the growth of *V. parahaemolyticus* B1-21 was significantly decreased at 5% NaCl as compared to that at 3% NaCl ($p < 0.05$) (Fig. S1, B), suggesting that *V. parahaemolyticus* B1-21 was less tolerant to the higher NaCl concentration. These results indicated that the *V. parahaemolyticus* isolates grew optimally in the TSB at 3% NaCl.

The pH of human stomach normally ranges pH 1-3, but can rise above 6.0 after food consumption (Sun et al. 2014). The acidic stomach condition challenges the bacterial pass through to the gastrointestinal tract where it colonizes and causes the diarrhea disease. Thus, we determined growth curves of the *V. parahaemolyticus* isolates in the TSB (3% NaCl) under the pH 6.0–8.5 conditions at 37 °C. As shown in Fig. S2 (A–E), the growth of all the isolates was inhibited under the acidic conditions (pH 6.0–6.5), whereas the neutral condition (pH 7.0) promoted the bacterial growth, and all the isolates grew vigorously at pH 7.5–8.5, showing the maximum biomass at pH 8.5 ($OD_{600} = 0.94$–1.20) at SGP. These results indicated that the *V. parahaemolyticus* isolates of aquatic animal origins grew optimally at pH 8.5, 3% NaCl in the TSB.

Growth curves of the *V. parahaemolyticus* isolates in the TSB (3% NaCl, pH 8.5) were also determined at 25 °C and 37 °C, respectively, wherein *V. parahaemolyticus* experiences during its life cycle in the environment and in the host. As shown in Fig. S3 (A–E), all the isolates could grow more exuberantly at 37 °C than at 25 °C. Therefore, the *V. parahaemolyticus* isolates were incubated in the TSB (pH 8.5, 3% NaCl) at 37 °C in the further analyses in this study, to avoid any condition influence other than the oxygen concentrations.

Growth of the *V. parahaemolyticus* isolates at different oxygen concentrations (21–5% O_2) was examined; and the results are presented in Fig. 1 A–E. Under the 5–10% O_2 conditions, the growth of all the isolates in the TSB (3% NaCl, pH 8.5) at 37 °C was repressed, and the maximum OD_{600} values ranged 0.40–0.52 at SGP. Under the 12% O_2 condition, all the isolates grew better than at 10% O_2. Upon the increased O_2 concentrations (15–21%), the *V. parahaemolyticus* isolates grew faster correspondingly, but reaching the maximum biomass ($OD_{600} = 0.90$–1.28) under the normal 21% O_2 condition. Additionally, we observed that the growth of *V. parahaemolyticus* ATCC17802 of the clinical origin was the slowest under the lower O_2 conditions among the test strains, moreover, it still showed the lower biomass under the 18% O_2 condition.

Effects of the hypoxic condition on biofilm formation of the *V. parahaemolyticus* isolates.

The ability of *Vibrio* to form biofilm attributes to their survival in the host and withstanding in different aquatic environments (Khan et al. 2020). Therefore, we asked whether and how the hypoxic condition (10% O_2) would affect biofilm formation of the *V. parahaemolyticus* isolates. The dynamic process of biofilm formation was monitored under the 10% O_2 condition when the isolates were incubated in the TSB (pH 8.5, 3% NaCl) at 37 °C for 60 h. As shown in Fig. 2A–E, the *V. parahaemolyticus* isolates formed biofilms at three different stages, including
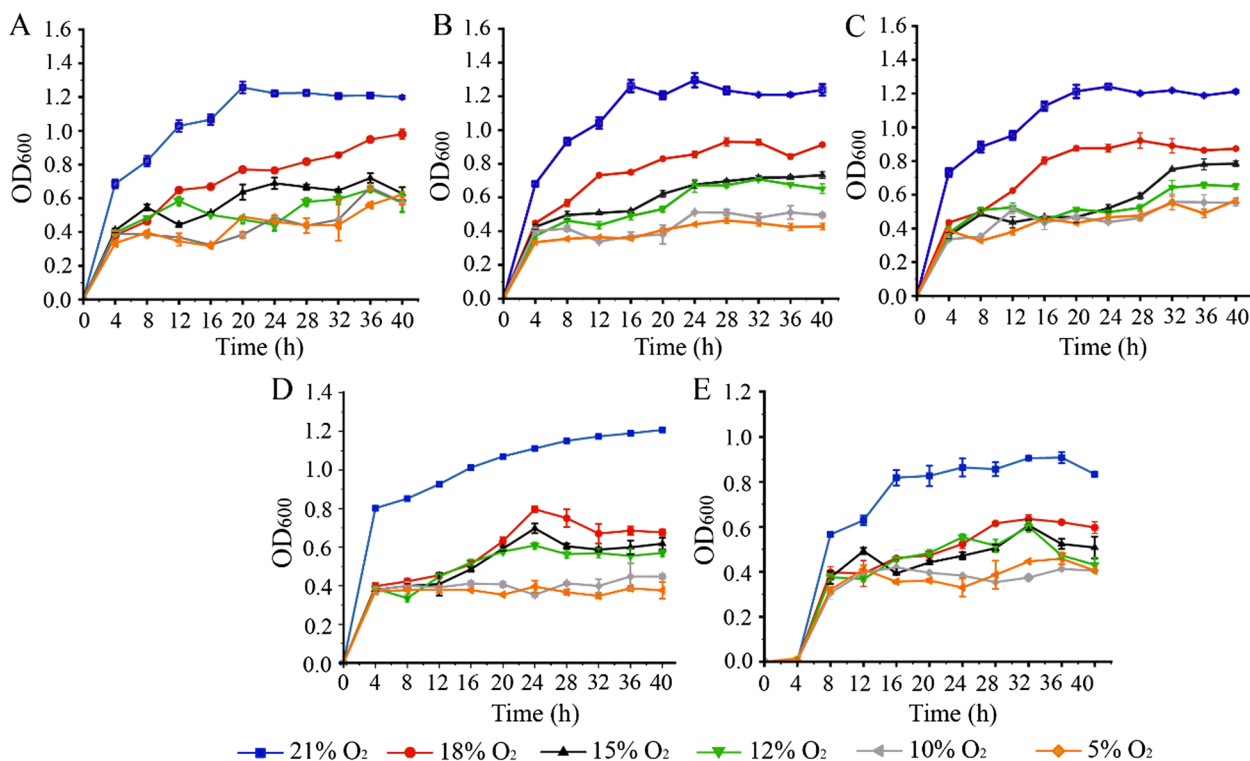
Fig. 1 The growth of the *V. parahaemolyticus* isolates in the TSB (pH 8.5, 3% NaCl) under different oxygen conditions at 37 °C. **A–E**: *V. parahaemolyticus* B8-26, *V. parahaemolyticus* B1-21, *V. parahaemolyticus* N2-5, *V. parahaemolyticus* L7-40, and *V. parahaemolyticus* ATCC17802, respectively

the development, maturation, and diffusion, similar to those under the normal 21% O_2 condition. However, different biofilm formation patterns were observed among the isolates.

Unexpectedly, under the 10% O_2 condition, the biofilm biomass generated by all the *V. parahaemolyticus* isolates was significantly increased at the development and maturation stages (0–36 h) as compared to those under the 21% O_2 condition ($p < 0.05$). The highest increase (2.70-fold) was observed in the *V. parahaemolyticus* B8-26 treatment group at 36 h ($p < 0.001$). Of note, the 10% O_2 condition significantly enhanced the biofilm formation of *V. parahaemolyticus* ATCC17802 for 48 h ($p < 0.05$) (Fig. 2, E). These results demonstrated that the hypoxic condition can enhance the biofilm formation of all the test *V. parahaemolyticus* isolates.

Cell morphological structure changes of the *V. parahaemolyticus* isolates under the hypoxic condition

Cell surface structure of the *V. parahaemolyticus* isolates under the hypoxic condition was further observed by the SEM assay. As shown in Fig. 3A–E, unexpectedly, in remarkable contrast to the control groups under the 21%

O_2 condition, whose cell surface structure was broken with obvious crumpling, rupture and cellular contents leakage after 24-h incubation, the *V. parahaemolyticus* isolates showed rod cells with slightly shrinkage on the cell surface after being treated with 10% O_2 for 24 h. Particularly, *V. parahaemolyticus* ATCC17802 cells in the control group were severely shrunk and deformed, whereas those in the hypoxia treatment group were rod-shaped and less destroyed in cell structure (Fig. 3, E). These results indicated that the 10% O_2 condition repressed the growth of the *V. parahaemolyticus* isolates. The cellular metabolisms-requiring O_2 were consequently down-regulated, thereby leading to the slower growth under the hypoxic condition.

Genome features of the *V. parahaemolyticus* isolates originating in edible aquatic animals

Based on the above results, draft genome sequences of *V. parahaemolyticus* B8-26, B1-21, N2-5, and L7-40 isolates of aquatic animal origins were determined, which yielded 37,042–51,777 clean sequencing reads. The assembled genome sizes were 4,913,675–5,353,490 bp with the GC contents of 45.29–45.44%. The yielded DNA scaffolds were 41–106. A total of 4,575–5,045 genes were
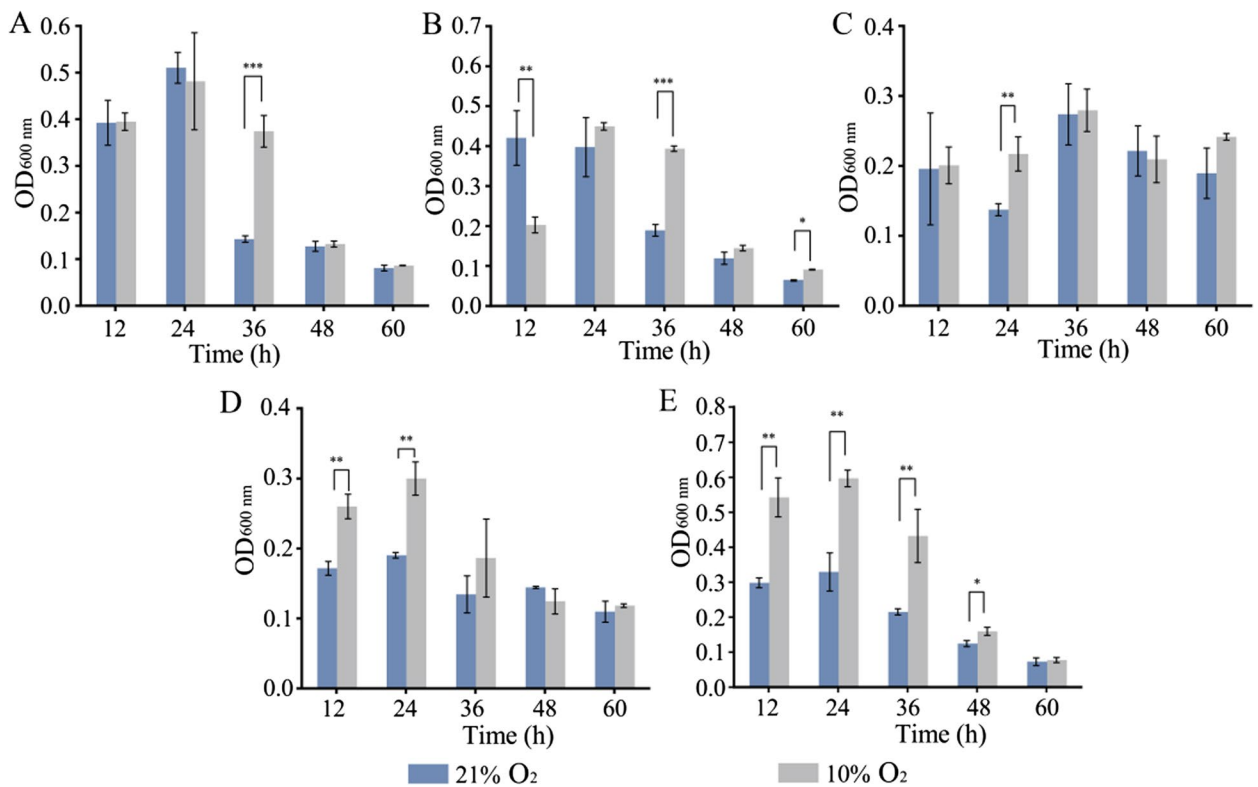
Fig. 2 The biofilm formation of the *V. parahaemolyticus* isolates grown in the TSB (pH 8.5, 3% NaCl) under the 21% O_2 and 10% O_2 conditions at 37 °C. **A–E**: *V. parahaemolyticus* B8-26, *V. parahaemolyticus* B1-21, *V. parahaemolyticus* N2-5, *V. parahaemolyticus* L7-40, and *V. parahaemolyticus* ATCC17802, respectively. *$p < 0.05$; **$p < 0.01$; ***$p < 0.001$
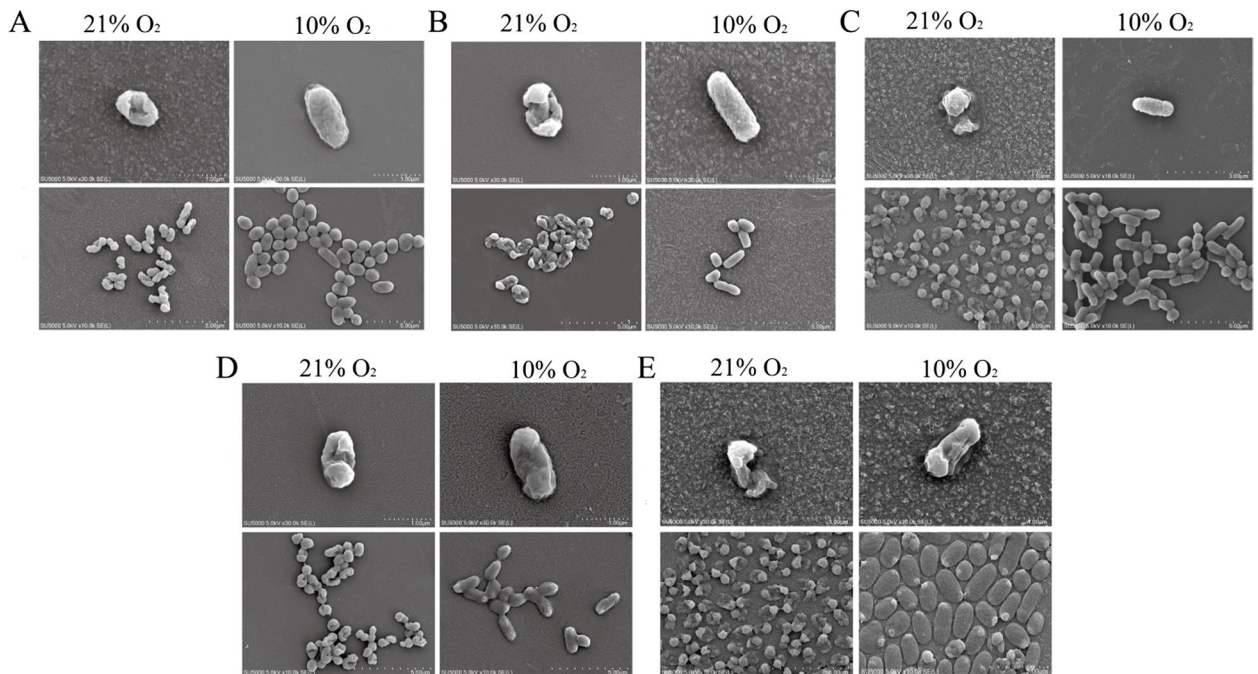

Fig. 3 The cell morphological structure of the *V. parahaemolyticus* isolates grown in the TSB (pH 8.5, 3% NaCl) under the 21% O_2 and 10% O_2 conditions at 37 °C for 24 h. **A–E**: *V. parahaemolyticus* B1-21, *V. parahaemolyticus* ATCC17802, *V. parahaemolyticus* B8-26, *V. parahaemolyticus* N2-5, and *V. parahaemolyticus* L7-40, respectively

Xu *et al. Annals of Microbiology*   (2024) 74:20

Page 8 of 23

predicted, of which the unknown function genes were 19.32–23.13% (Table 2, Fig. S4).

V. parahaemolyticus B8-26, B1-21, N2-5, and L7-40 genomes also carried putative mobile genetic elements (MGEs), such as genome islands (GIs, $n = 36$), prophages ($n = 4$), integrons (INs, $n = 26$), and insertion sequences (ISs, $n = 12$), suggesting possible horizontal gene transfer (HGT) during the *V. parahaemolyticus* genome evolution. The draft genomes of *V. parahaemolyticus* B8-26, B1-21, N2-5, and L7-40 isolates were deposited in the GenBank database under the accession numbers JAO-DUR000000000, JAOPTY000000000, JAODVT000000000, and JAODVU000000000, respectively.

Additionally, based on the draft genome of *V. parahaemolyticus* ATCC17802 in the GenBank database (accession numbers NZ_CP014046.2) (Yang et al. 2015), we also identified several MGEs, including GIs ($n = 2$), and INs ($n = 7$) in this isolate.

GIs

GIs can shape bacterial genomes and affect bacterial fitness to the environment (Ghazali et al. 2021). In this study, 36 GIs were identified in the four *V. parahaemolyticus* genomes of aquatic animal origins, which contained 3–14 GIs with 5,572–38,679 bp, and carried 7–45 predicted genes with diverse biological functions (Fig. 4, Table S3).

The *V. parahaemolyticus* N2-5 genome contained the maximum number of GIs ($n = 14$, GIs 1–14), which were 5,572–38,427 bp, with 7–33 predicted genes. Conversely, the *V. parahaemolyticus* B8-26 genome carried the fewest GIs ($n = 3$, GIs 1–3), ranging 13,548–38,679 bp with 19–34 predicted genes. Notably, there were some GIs carrying virulence-related genes. For example, the GI 3 in *V. parahaemolyticus* B8-26, and the GI 11 in *V. parahaemolyticus* N2-5, encoding type II toxin-antitoxin (TA) system prophylactic-host death family antitoxins (*Vp B8-26_3404*, *Vp N2-5_3709*). The TA systems are involved in biofilm formation, persistence, stress endurance, and programmed cell death in favor of bacterial population (Hosseini et al. 2019).

Prophages

Phages, being the most abundant biological entities on earth, are viruses that infect bacteria, and constantly reshape bacterial communities (Wahl et al. 2019). In this study, we found four prophages in the *V. parahaemolyticus* B1-21, N2-5, and L7-40 genomes (Table S4), ranging 11,738–32,968 bp with 14–47 genes (Fig. 5). Like *V. parahaemolyticus* B8-26, no prophage was reported in *V. parahaemolyticus* ATCC17802 (Yang et al. 2015).

V. parahaemolyticus B1-21 genome contained two prophage gene clusters that showed high sequence similarity to *Vibrio*_phage_K139 (33,106 bp, NCBI accession number: NC_003313), and *Vibrio*_phage_fs2 (8,651 bp, NCBI accession number: NC_001956), respectively. The *Vibrio*_phage_K139 homologue was also found in the *V. parahaemolyticus* L7-40 genome, but with a truncated version (18,896 bp) carrying 23 genes, suggesting the rearrangement of *Vibrio*_phage_K139 during the *V. parahaemolyticus* genome evolution. The *V. parahaemolyticus* N2-5 genome
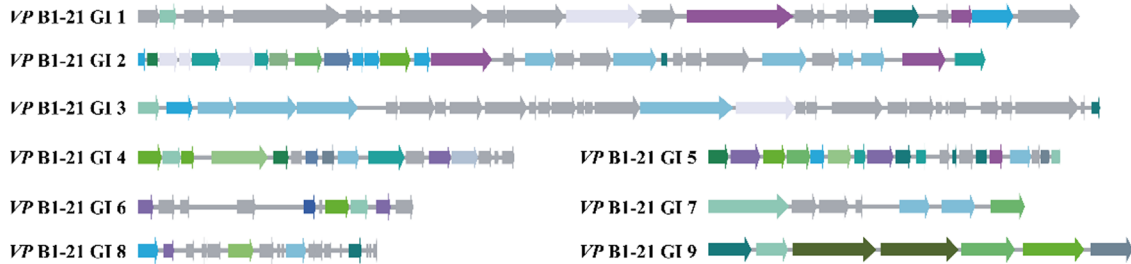
Table 2 Genome features of the *V. parahaemolyticus* isolates used in this study

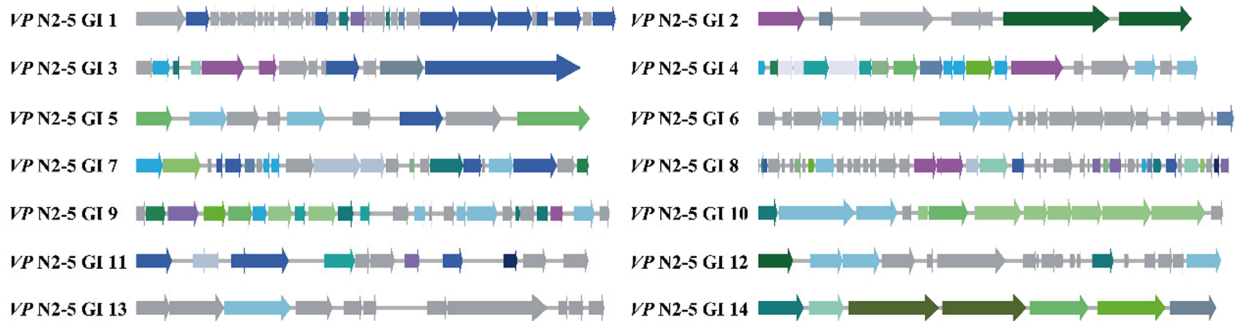| Genome feature	*V. parahaemolyticus* strain				
	B8-26	**B1-21**	**N2-5**	**L7-40**	**ATCC17802**
Genome size (bp)	4,975,325	4,989,057	5,353,490	4,913,675	4,922,919
Clean reads	46,461	37,042	51,777	40,135	36,398
G + C (%)	45.38	45.41	45.29	45.44	45.43
DNA Scaffold	52	41	62	106	69
Total predicted gene	4,575	4,597	5,045	4,600	4,565
Protein-coding gene	4,458	4,496	4,924	4,490	4,449
RNA gene	57	54	56	60	53
Genes assigned to COG	3,723	3,712	3,878	3,683	3,693
GI	3	9	14	10	2
Prophage	0	2	1	1	0
CRISPR-Cas	0	1	1	3	4
IN	5	11	8	2	7
IS	4	1	5	2	0
GenBank accession no	JAODUR000000000	JAOPTY000000000	JAODVT000000000	JAODVU000000000	NZ_CP014046.2
Source	This study	This study	This study	This study	(Yang et al. 2015)

Fig. 4 Gene organizations of the GIs identified in the *V. parahaemolyticus* genomes. Different colors referred to COG functional classification and genes with unknown function were in grey

contained a truncated version (29,468 bp) of *Enterobacteria*_phage_Mu (36,717 bp, NCBI accession number: NC_000929), carrying 47 genes encoding 32 unknown proteins, which suggested possible transmission of the *Enterobacteria*_phage_Mu between the *Vibrio* and *Enterobacteria* genera pathogens.
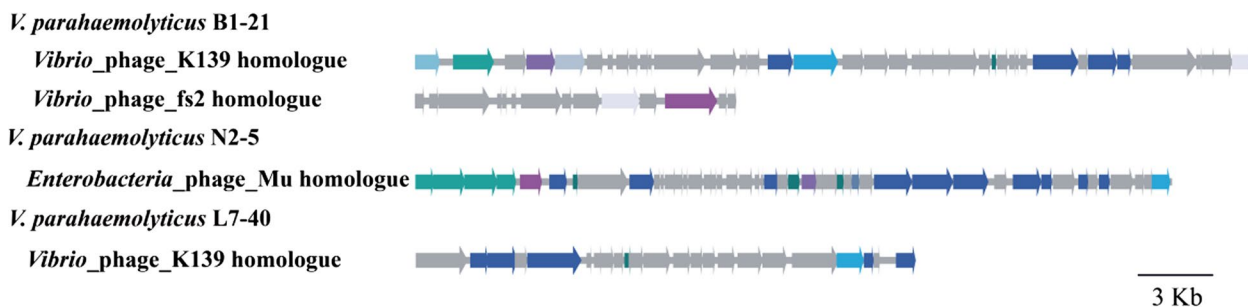
Fig. 5 The structure diagram of the prophages identified in the *V. parahaemolyticus* genomes

INs

INs are also critically involved in bacterial evolution and antimicrobial resistance with the carried gene cassettes (Ali et al. 2022). In this study, all the *V. parahaemolyticus* genomes contained INs (n = 2–11) ranging 605 bp–65,657 bp (Fig. S5-Fig. S6, Table S5).

The *V. parahaemolyticus* B1-21 genome contained the maximum number of INs (n = 11, INs 1–11), but all of which were incomplete INs with gene cassettes. In contrast, the *V. parahaemolyticus* L7-40 genome carried only two INs (INs 1–2), including one complete IN (IN 1) and one gene cassette (IN 2). Additionally, seven INs were identified in the *V. parahaemolyticus* ATCC17802 genome, including one complete (IN 1) with an integrase *IntI* 4 (*Vp B8-26_1368*), suggesting that the IN 1 was a super integron (Yang et al. 2015).

ISs

ISs are mobile repeat sequences that can copy themselves to new locations in bacterial genomes (Tempel et al. 2022). In this study, ISs were identified in the *V. parahaemolyticus* B8-26 (n = 4), B1-21 (n = 1), N2-5 (n = 5), and L7-40 (n = 2) genomes (Table S6), but absent in *V. parahaemolyticus* ATCC17802 (Yang et al. 2015). Notably, one IS001 (1,307 bp) belonging to the ISAs1 family was identified in *V. parahaemolyticus* L7-40, encoding a c-di-GMP metabolism protein (*Vp L7-40_4574*), which is critical to bacterial adaptation to changing environments, including biofilm formation, host colonization and virulence (Kumar and Chatterji 2008).

Putative virulence and resistance-associated genes

Many virulence-related genes (n = 42–45) were identified in the *V. parahaemolyticus* B8-26, B1-21, N2-5, and L7-40 genomes. For instance, more than thirty genes for type III secretion system 1 (T3SS1) were found, encoding the VecA, TyeA, SycN, YscO, VcrDGHRV, VopBDNQRS, and VscBCDFGHIJKLNQRSTUXY. The ExsA gene was also found in these genomes (*Vp B8-26_3495, Vp B1-21_3659, Vp N2-5_3801,* and *Vp L7-40_3386*), which

is the master transcription factor that positively regulates T3SS1 expression (Gu et al. 2020). In addition, *V. parahaemolyticus* ATCC17802 has both T3SS1 and T3SS2, and TRHs (Yang et al. 2015).

Several antibiotic resistance-related genes (n = 3) and heavy metal tolerance-ralated genes (n = 8) were identified in the *V. parahaemolyticus* B8-26, B1-21, N2-5, L7-40, and ATCC17802 genomes (Table 3), which provided the genome-wide evidence for resistance phenotypes of the *V. parahaemolyticus* isolates.

Comparative transcriptome analysis of the *V. parahaemolyticus* isolates in response to the hypoxic condition

Based on the *V. parahaemolyticus* B8-26, B1-21, N2-5, L7-40 genomes determined in this study, coupled with the *V. parahaemolyticus* ATCC17802 genome, we further examined genome-wide gene expression changes triggered by the hypoxic condition. The isolates were incubated in the TSB under the 10% O_2 condition at 37 °C for 24 h, at which the cell morphological structure changes of the *V. parahaemolyticus* isolates was the most obvious, therefore, their transcriptomes were determined. The complete lists of DEGs in the *V. parahaemolyticus* isolates are available in the NCBI SRA database (https://

Table 3 The antibiotic and heavy metal resistance-related genes identified in the *V. parahaemolyticus* genomes

Antibiotic / heavy metal	Gene	*V. parahaemolyticus* isolate
Fluoroquinolone	*crp*	B8-26, B1-21, N2-5, L7-40, ATCC17802
Tetracycline	*Tet (35)*	B8-26, B1-21, N2-5, L7-40, ATCC17802
Beta-lactam	*bla*$_{CARB-18}$	B8-26, B1-21, N2-5, L7-40, ATCC17802
Heavy metal	*cusARS*	B8-26
Heavy metal	*dsbABC*	B8-26, N2-5
Heavy metal	*smtA*	B8-26, B1-21, L7-40, ATCC17802
Heavy metal	*zntA*	B8-26, B1-21, L7-40, ATCC17802

Xu *et al. Annals of Microbiology* (2024) 74:20

Page 11 of 23

under the accession number PRJNA906699 and PRJNA767551.

The major altered metabolic pathways in *V. parahaemolyticus* B8-26 triggered by the hypoxic condition

Approximately 65.89% (2,722/4,131) of *V. parahaemolyticus* B8-26 genes were expressed differently under the hypoxic condition as compared to the control group. Among these, 413 differently expressed genes (DEGs) showed higher transcription levels (fold change, $FC \geq 2.0$), whereas 2,309 DEGs were down-regulated ($FC \leq 0.5$). The comparative transcriptomic analysis revealed fourteen significantly changed metabolic pathways, including the aminoacyl-tRNA biosynthesis; protein export; peptidoglycan (PG) biosynthesis; citrate cycle; sulfur metabolism; ubiquinone and other terpenoid-quinone biosynthesis;, RNA degradation; glyoxylate and dicarboxylate metabolism; purine metabolism; thiamine metabolism; ATP-binding cassette (ABC) transporters; pyruvate metabolism; tyrosine metabolism; and carbon fixation pathways in prokaryotes (Fig. 6, Table S7).

Remarkably, all DEGs in the aminoacyl-tRNA biosynthesis ($n = 25$), PG biosynthesis ($n = 17$), citrate cycle

($n = 8$), and ubiquinone and other terpenoid-quinone biosynthesis ($n = 17$) were significantly repressed at the transcription levels in *V. parahaemolyticus* B8-26 under the hypoxic condition (0.015–fold to 0.497–fold) ($p < 0.05$). Aminoacyl-tRNA synthetases are essential for protein synthesis (Rubio Gomez and Ibba 2020). The expression of many such enzymes and proteins was repressed in *V. parahaemolyticus* B8-26. For instance, the DEG encoding an alanyl-tRNA editing protein (*Vp_B8-26_03025*) was strongly inhibited (0.080–fold), suggesting that the stringent response shut down the translation to avoid toxic generation of mistranslated/misfolded proteins (Aggarwal et al. 2021). As the major component of bacterial cell wall, the biosynthesis of PG is closely related to cell wall growth and turnover (Wamp et al. 2020). In this study, seventeen DEGs involved in the PG biosynthesis were inhibited under the hypoxic condition. For example, the DEG encoding a D-alanyl-D-alanine carboxypeptidase (*Vp_B8-26_24445)* was significantly down-regulated (0.448–fold), which is involved in the reconstruction of newly synthesized PG in *Francisell*a (Spidlova et al. 2018). The citrate cycle (Krebs cycle) is a major aerobic pathway for the final stages of carbohydrate and fatty acid
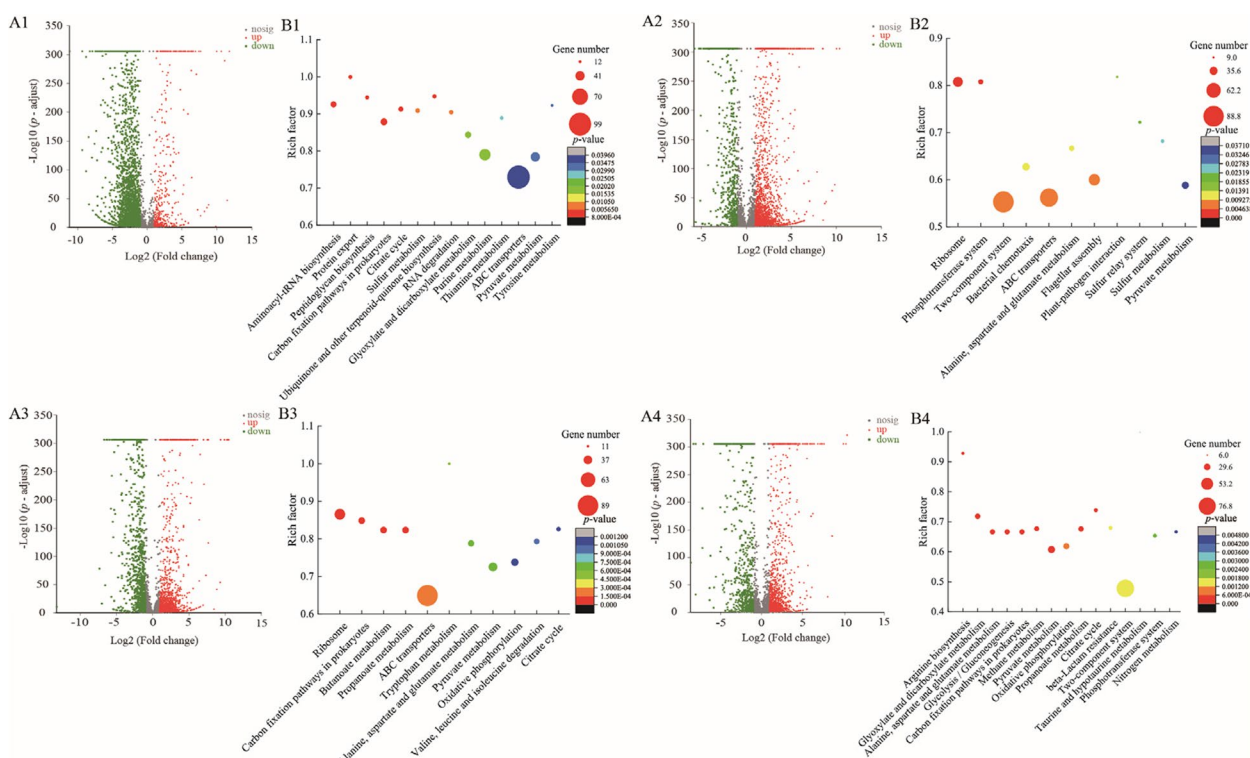

Fig. 6 The Volcano plot of differential gene expression (**A**), and the major changed metabolic pathways (**B**) in *V. parahaemolyticus* strains under the hypoxic condition (10% O$_2$). **A**: The X and Y axes represented changes of the up/down-regulated genes, and the corresponding significant differences, respectively. **B** The X and Y axes represented the major changed metabolic pathways in *V. parahaemolyticus* strains under the hypoxic condition, and the ratios of the number of DEGs in the metabolic pathways to the total number of DEGs in all metabolic pathways. A1 and B1, A2 and B2, A3 and B3, A4 and B4: *V. parahaemolyticus* B8-26, B1-21, N2-5, and L7-40 strains, respectively

Xu *et al. Annals of Microbiology*   (2024) 74:20

Page 12 of 23

oxidation, which provides NADH to be used for oxidative phosphorylation and other metabolic reactions. In this study, eight DEGs in the citrate cycle were down-regulated as well. For instance, the DEG encoding a malate dehydrogenases (MDH) *(Vp_B8-26_01555)* was strongly down-regulated (0.022–fold). The MDH catalyzes the NAD/NADH-dependent interconversion of malate and oxaloacetate. The malate/aspartate of this reaction is involved in tricarboxylic acid cycle (Minárik et al. 2002). Additionally, among the seventeen down-regulated DEGs in the ubiquinone and other terpenoid-quinone biosynthesis, the DEG encoding a NAD(P)H quinone oxidoreductase (NQO) (*Vp_B8-26_12250*) was significantly repressed (0.172–fold), which is a two-electron reductase responsible for detoxification of quinones and bioactivation of certain quinones (Zhang et al. 2018). These results signified that the hypoxic condition likely inhibited protein translation, bacterial cell wall synthesis, and energy supply in *V. parahaemolyticus* B8-26.

Sulfur is also a requirement for both the host and colonizing bacteria (Kies et al. 2022). In this study, fourteen DEGs were significantly down-regulated in the sulfur metabolism in *V. parahaemolyticus* B8-26 under the hypoxic condition (0.010–fold to 6.247–fold) ($p < 0.05$). For example, the NrfD-like subunits are found in many diverse membrane complexes, which may participate in the metabolism of oxygen, nitrogen, sulfur, arsenate or hydrogen (Calisto and Pereira 2021). Nevertheless, in this study, the expression of NrfD (*Vp_B8-26_10960*) was strongly down-regulated (0.007–fold), suggesting the inhibited sulfur metabolism, thereby energy conversion in *V. parahaemolyticus* B8-26 under the hypoxic condition.

Of note, approximately 85 DEGs in the ABC transport were also significantly inhibited in *V. parahaemolyticus* B8-26 under the hypoxic condition (0.003–fold to 0.498–fold) ($p < 0.05$). The ATP-dependent ABC transporter proteins facilitate the import and/or export of various substrates, including lipids, sugars, amino acids and peptides, ions, and drugs (Thurm et al. 2021). For example, the DEG encoding the ATP-binding cassette domain-containing protein (*Vp_B8-26_06880*) was greatly down-regulated (0.003–fold), which contains two domains capable of ATP hydrolysis in order to fuel protein function (Alqahtani et al. 2019). The down-regulation of the ABC transport suggested the inactive cellular transport function under the hypoxia, which likely led to harmful substance accumulate and retarded bacterial growth.

Conversely, the expression of some DEGs was significantly increased in *V. parahaemolyticus* B8-26 under the hypoxic condition ($p < 0.05$). For instance, four DEGs involved in the protein export were significantly up-regulated (2.201–fold to 7.248–fold) ($p < 0.05$), e.g., the protein translocase subunit SecD (*Vp_B8-26_23120*, 7.248-fold), and protein translocase subunit SecF (*Vp_B8-26_23115*, 5.060-fold). The SecDF belong to the SecYEG-SecDF-YajC-YidC holo-translocon (HTL) protein secretase/insertase, a supercomplex necessary for protein secretion, insertion membrane and complex assembly (Komar et al. 2016).

Taken, the comparative transcriptome data revealed fourteen significantly changed metabolic pathways in *V. parahaemolyticus* B8-26 under the hypoxic condition. Notably, the down-regulated protein translation and transport, ABC transporters, bacterial cell wall synthesis and energy conversion likely contributed to the retarded cell growth of *V. parahaemolyticus* B8-26 under the hypoxic condition.

The major changed metabolic pathways in *V. parahaemolyticus* B1-21 triggered by the hypoxic condition

Approximately 46.77% (2,058/4,400) of *V. parahaemolyticus* B1-21 genes were expressed differently under the hypoxic condition as compared to the control group. Of these, 1,533 DEGs were up-regulated (FC ≥ 2.0), whereas 525 DEGs were down-regulated (FC ≤ 0.5). Eleven significantly changed metabolic pathways were identified, including the ribosome; phosphotransferase system (PTS); two-component system (TCS); bacterial chemotaxis; ABC transporters; alanine, aspartate and glutamate metabolism; flagellar assembly; plant-pathogen interaction; sulfur relay system; sulfur metabolism; and pyruvate metabolism (Fig. 6, Table S8).

Bacterial chemotaxis is a critical ability to search for the optimal environment to ensure the survival of bacterial species (Jeong 2021). Three DEGs in the bacterial chemotaxis were significantly repressed in *V. parahaemolyticus* B1-21 under the hypoxic condition (0.188–fold to 0.465–fold) ($p < 0.05$), including a chemotactic protein Chew (*Vp_B1-21_11985*), a flagellar motor switch protein (*Vp_B1-21_12100*), and a chemotactic response regulator protein-glutamate methylase (*Vp_B1-21_12000*). For example, the DEG encoding the CheW (*Vp_B1-21_11985*), which is involved in the transmission of sensory signals from the chemoreceptors to the flagellar motors (Rosario et al. 1994), was significantly repressed (0.465–fold). Meanwhile, the DEG encoding the flagellar motor switch protein (*Vp_B1-21_12100*) was also highly repressed (0.188–fold). These results indicated the down-regulated bacterial chemotaxis under the hypoxic condition, thereby inhibiting bacterial migration to the environment conducive to survival.

Approximately 28 DEGs in the TCS were significantly inhibited (0.053–fold to 0.494–fold), whereas 56 DEGs

Xu *et al. Annals of Microbiology*   (2024) 74:20

Page 13 of 23

were significantly enhanced (2.017–fold to 0.494–fold) at the transcriptional levels in *V. parahaemolyticus* B1-21 under the hypoxic condition ($p < 0.05$). Bacteria sense and respond to environmental changes via TCS, e.g., cell surface modifications, and increased biofilm formation (Tierney and Rather 2019). For example, the DEG encoding an acetyl coenzyme A acetyltransferase (ACAT) (*Vp_B1-21_23095*, 0.121–fold) was significantly inhibited in *V. parahaemolyticus* B1-21 ($p < 0.05$), which catalyzes the reversible formation of acetylacyl coenzyme A from two acetyl coenzyme A molecules during the ketogenesis and ketolysis (Goudarzi 2019).

Remarkably, all DEGs ($n = 42$) in the ribosome were significantly down-regulated (0.214–fold to 0.495–fold) in *V. parahaemolyticus* B1-21 under the hypoxic condition ($p < 0.05$), e.g., 50S ribosomal proteins (*Vp_B1-21_01230, Vp_B1-21_06585, Vp_B1-21_13890*), and 30S ribosomal proteins (*Vp_B1-21_01360, Vp_B1-21_11045, Vp_B1-21_15475, Vp_B1-21_15315*). Ribosomes are essential for protein production, and thus for bacterial growth, and proliferation (Turi et al. 2019). These results indicated that *V. parahaemolyticus* B1-21 reduced protein translation in response to the hypoxic condition.

Conversely, all DEGs ($n = 21$) in the PTS were significantly up-regulated (2.616–fold to 28.083–fold) in *V. parahaemolyticus* B1-21 under the hypoxic condition ($p < 0.05$). For instance, the gene encoding a fused PTS fructose transporter subunit IIA/HPr protein (*Vp_B1-21_21185*) was highly up-regulated (28.083–fold), suggesting the up-regulated transport and utilization of carbohydrates in *V. parahaemolyticus* B1-21 under the hypoxic condition.

Similar to *V. parahaemolyticus* B8-26, the ABC transporters, sulfur metabolism, and pyruvate metabolism were also significantly changed in *V. parahaemolyticus* B1-21 under the hypoxic condition.

Taken together, the comparative transcriptome data revealed eleven significantly changed metabolic pathways in *V. parahaemolyticus* B1-21 under the hypoxic condition. Specially, *V. parahaemolyticus* B1-21 reduced protein translation, but enhanced transport and utilization of carbohydrates in response to the hypoxic condition.

The major changed metabolic pathways in *V. parahaemolyticus* N2-5 triggered by the hypoxic condition

Approximately 47.55% (783/4,400) of *V. parahaemolyticus* N2-5 genes were expressed differently under the hypoxic condition as compared to the control group. Of these, 1,102 DEGs were up-regulated (FC ≥ 2.0), whereas 965 DEGs were down-regulated (FC ≤ 0.5). Eleven significantly changed metabolic pathways were identified, including ABC transporters; the ribosome; butanoate metabolism; tryptophan metabolism; alanine, aspartate and glutamate

metabolism; propanoate metabolism; pyruvate metabolism; oxidative phosphorylation; valine, leucine and isoleucine degradation; citrate cycle; and carbon fixation pathways in prokaryotes (Fig. 6, Table S9).

The same case as *V. parahaemolyticus* B1-21, all DEGs ($n = 45$) in the ribosomes were significantly down-regulated (0.137–fold to 0.468–fold) at the transcription levels in *V. parahaemolyticus* N2-5 under the hypoxic condition ($p < 0.05$). Like *V. parahaemolyticus* B8-26, all DEGs ($n = 5$) in the citrate cycle were also significantly repressed (0.040–fold to 0.188–fold) in *V. parahaemolyticus* N2-5.

Of note, almost all DEGs ($n = 24$) in the oxidative phosphorylation were significantly repressed (0.062–fold to 0.497–fold) in *V. parahaemolyticus* N2-5 under the hypoxic condition ($p < 0.05$), e.g., the F0F1 ATP synthase subunits A, B, α, β, and γ (*Vp_N2-5_16940, Vp_N2-5_16930, Vp_N2-5_16920, Vp_N2-5_16910*, and *Vp_N2-5_16915*), a cytochrome o ubiquinol oxidase subunit I (*Vp_N2-5_20305*), a cytochrome d ubiquinol oxidase subunit II (*Vp_N2-5_05315*), a cytochrome o ubiquinol oxidase subunit III (*Vp_N2-5_20310*), a cytochrome ubiquinone oxidase (*Vp_N2-5_05315*), a cytochrome c1, a cytochrome bc complex cytochrome b subunit (*Vp_N2-5_02185*), and a protoheme IX farnesyltransferase (*Vp_N2-5_20320*). The oxidative phosphorylation provides most of the ATP that is required for setting and maintaining cellular metabolic homeostasis (Wilson 2017). The significant repressed oxidative phosphorylationof indicated insufficient cellular energy production in *V. parahaemolyticus* N2-5, consequently affecting energy expenditure and cell growth under the hypoxic condition.

In the butanoate metabolism, thirteen DEGs were significantly down-regulated (0.028–fold to 0.475–fold) in *V. parahaemolyticus* N2-5 ($p < 0.05$), whereas five DEGs were significantly up-regulated (3.077–fold to 14.428–fold) ($p < 0.05$). For example, the DEG encoding a class I poly(R)-hydroxyalkanoic acid (PHA) synthase (*Vp_N2-5_23085*) was highly down-regulated (0.028–fold). PHAs are aliphatic polyesters produced by many bacteria and archaea in response to various environmental conditions (McCool and Cannon 2001).

In the tryptophan metabolism, three DEGs were significantly down-regulated (0.033–fold to 0.347–fold) in *V. parahaemolyticus* N2-5 ($p < 0.05$), whereas two DEGs were significantly up-regulated (8.781–to 10.778–fold) ($p < 0.05$). Of these, the expression of a catalase (*Vp_N2-5_23615*) was highly up-regulated (8.781–fold). The catalase decomposes hydrogen peroxide, protecting cells from potentially harmful reactive oxygen species (Kim et al. 2018).

Similar to *V. parahaemolyticus* B1-21, the ABC transport, and alanine, aspartate and glutamate metabolism

were significantly changed in *V. parahaemolyticus* N2-5 as well.

Taken, the comparative transcriptome analysis revealed eleven significantly changed metabolic pathways in *V. parahaemolyticus* N2-5 under the hypoxic condition, some of which were also altered in *V. parahaemolyticus* B1-21 and *V. parahaemolyticus* B8-26. Specially, the protein translation, citrate cycle, propionate metabolism, oxidative phosphorylation, carbon fixation pathways in prokaryotes, and valine, leucine and isoleucine degradation were all repressed in *V. parahaemolyticus* N2-5 for growth under the hypoxic condition.

The major changed metabolic pathways in *V. parahaemolyticus* L7-40 triggered by the hypoxic condition

Approximately 37.43% (783/4,400) of *V. parahaemolyticus* L7-40 genes were expressed differently under the hypoxic condition as compared to the control group. Of these, 1,032 DEGs were up-regulated (FC $\geq$ 2.0), whereas 615 DEGs were repressed (FC $\leq$ 0.5). Fifteen significantly changed metabolic pathways were identified, including the arginine biosynthesis; glyoxylate and dicarboxylate metabolism; glycolysis/gluconeogenesis; methane metabolism; alanine, aspartate and glutamate metabolism; pyruvate metabolism; oxidative phosphorylation; propanoate metabolism; citrate cycle; beta-lactam resistance; TCS; taurine and hypotaurine metabolism; PTS; nitrogen metabolism; and carbon fixation pathways in prokaryotes (Fig. 6, Table S10).

Like *V. parahaemolyticus* B8-26, and N2-5 strains, all DEGs ($n=5$) in the citrate cycle were significantly down-regulated (0.106–fold to 0.471–fold) in *V. parahaemolyticus* L7-40 under the hypoxic condition ($p < 0.05$). For example, the DEG encoding a fumarate reductase (*Vp_L7-40_15840*) was significantly inhibited (0.471–fold) ($p < 0.05$), which is a flavin protease containing the cofactor flavin adenine dinucleotide and reduces fumarate to succinate (Alqahtani et al. 2019). Fumarate reductases are essential for maintaining redox homeostasis in cells because they reoxidize intracellular flavin adenine dinucleotides (FADH$_2$) under the hypoxic conditions (Kim et al. 2018). The DEG encoding a succinate dehydrogenase (SDH) (*Vp_L7-40_15845*) was also inhibited (0.111–fold) ($p < 0.05$), which is a critical enzyme involved in the tricarboxylic acid cycle and oxidative phosphorylation for energy production (Moosavi et al. 2019). These results suggested that the hypoxia likely disrupted the cellular redox balance and the energy supply in *V. parahaemolyticus* L7-40.

Like *V. parahaemolyticus* N2-5, all DEGs ($n=14$) in the propanoate metabolism were significantly down-regulated (0.121–fold to 0.437–fold) in *V. parahaemolyticus* L7-40 ($p < 0.05$). The same case as *V. parahaemolyticus* N2-5,

the 16 of 21 DEGs in the oxidative phosphorylation were significantly down-regulated (0.116–fold to 0.454–fold) as well ($p < 0.05$). Interestingly, in marked contrast to the most inhibited DEGs in the oxidative phosphorylation, the expression of one DEG encoding a manganese-dependent inorganic pyrophosphatase (PPase, *Vp_L7-40_09185*), which plays an essential role in the conservation of energy and supplies energy for numerous biosynthetic pathways (Hu et al. 2020), was strongly up-regulated (33.120–fold) in *V. parahaemolyticus* L7-40 ($p < 0.05$).

In the glyoxylate and dicarboxylate metabolism, the 20 of 24 DEGs were significantly down-regulated (0.019–fold to 0.491–fold) in *V. parahaemolyticus* L7-40 under the hypoxic condition ($p < 0.05$). Of these, the DEG encoding an acetate-CoA ligase (*Vp_L7-40_16020*) was highly down-regulated (0.019–fold). Acetyl-CoA is a vitally important and versatile metabolite used for many cellular processes, and can also deal with stress such as low nutritional availability and hypoxia (Miller et al. 2021).

Similar to *V. parahaemolyticus* B1-21, all DEGs ($n=13$) in the PTS were significantly up-regulated (2.338–fold to 64.585–fold) in *V. parahaemolyticus* L7-40 under the hypoxic condition ($p < 0.05$). In the glycolysis/gluconeogenesis, the 17 of 21 DEGs were significantly up-regulated (2.199–fold to 10.689–fold) in *V. parahaemolyticus* L7-40 ($p < 0.05$). Of these, the DEG encoding a 6-phosphofructokinase (PFK, *Vp_L7-40_15910*) was highly up-regulated (10.689–fold). The PFK is one of the most prominent rate-limiting enzymes in the glycolytic pathway. The increase in glycolytic flux is beneficial for maintaining bioenergetic homeostasis during the hypoxia (Kierans and Taylor 2021).

In addition, similar to *V. parahaemolyticus* B8-26, and *V. parahaemolyticus* N2-5, the TCS, pyruvate metabolism, as well as alanine, aspartate and glutamate metabolism were also significantly changed in *V. parahaemolyticus* L7-40 under the hypoxic condition.

Taken, the comparative transcriptome analysis revealed fifteen significantly changed metabolic pathways in *V. parahaemolyticus* L7-40, some of which were also identified in *V. parahaemolyticus* B8-26, N2-5, and B1-21 isolates under the hypoxic condition. Specifically, *V. parahaemolyticus* L7-40 inhibited the glyoxylate and dicarboxylate metabolism, but up-regulated the glycolysis/gluconeogenesis, and changed the nitrogen metabolism, and the arginine biosynthesis in response to the hypoxic condition.

The major changed metabolic pathways in *V. parahaemolyticus* ATCC17802 triggered by the hypoxic condition

Approximately 57.12% (783/4,674) of *V. parahaemolyticus* ATCC17802 genes were expressed differently under

the hypoxic condition as compared to the control group. Among these, 361 DEGs were up-regulated (FC ≥ 2.0), whereas 2,309 DEGs were down-regulated (FC ≤ 0.5). Ten significantly changed metabolic pathways were identified, including the ribosome; ABC transporters; aminoacyl-tRNA biosynthesis; oxidative phosphorylation; pyrimidine metabolism; fatty acid biosynthesis; arginine and proline metabolism; lipopolysaccharide (LPS) biosynthesis; purine metabolism, and carbon fixation pathways in prokaryotes (Fig. 7, Table S11).

Similar to *V. parahaemolyticus* B1-21, and N2-5 isolates, all DEGs ($n = 49$) in the ribosome were significantly down-regulated (0.033–fold to 0.243–fold) at the transcriptional level in *V. parahaemolyticus* ATCC17802 under the hypoxic condition ($p < 0.05$). The same case as *V. parahaemolyticus* N2-5, and L7-40 isolates, all DEGs ($n = 35$) in the oxidative phosphorylation were significantly down-regulated (0.029–fold to 0.440–fold) in *V. parahaemolyticus* ATCC17802, except the polyphosphate kinase (*Vp_17802_02840*, 2.187–fold).

In the fatty acid biosynthesis, all DEGs ($n = 17$) were significantly down-regulated (0.047–fold to 0.427–fold) in *V. parahaemolyticus* ATCC17802 ($p < 0.05$). Fatty acid biosynthesis plays a central role in building cell membrane, reserving cell energy, and production of precursors to second messenger molecules (Günenc et al. 2022). For instance, the DEG encoding a trans-2-enoyl-CoA

reductase family protein (*Vp_17802_21460*) was strongly down-regulated (0.047–fold) in *V. parahaemolyticus* ATCC17802, which is involved in chain lengthening of fatty acids (Uchida et al. 2021).

In the LPS biosynthesis, most DEGs (16/18) were significantly down-regulated (0.068–fold to 0.476–fold) in *V. parahaemolyticus* ATCC17802 ($p < 0.05$). The LPS, the major component of the outer membrane of Gram-negative bacteria, is essential for bacterial viability and host–pathogen interactions (Kutschera et al. 2021). For instance, the DEG encoding the tetraacyldisaccharide 4′-kinase (*Vp_17802_04990*) was strongly down-regulated (0.068–fold) in *V. parahaemolyticus* ATCC17802, which is the prime enzyme for lipid biosynthesis vital for bacterial survival (Damale et al. 2022).

In the pyrimidine metabolism, most DEGs (26/30) were significantly down-regulated (0.026–fold to 0.450–fold) in *V. parahaemolyticus* ATCC17802 ($p < 0.05$). Pyrimidines are structural elements of a wide range of essential compounds in the synthesis of DNA, RNA, lipids, and carbohydrates (Garavito et al. 2015). For instance, the DEG encoding a thymidine kinase (TK, *Vp_17802_05700*) was strongly down-regulated (0.051–fold) in *V. parahaemolyticus* ATCC17802. The TK is involved in the pyrimidine nucleotide recovery pathway, a cell-proliferation marker (Fanelli et al. 2021). Interestingly, among the four up-regulated DEGs in
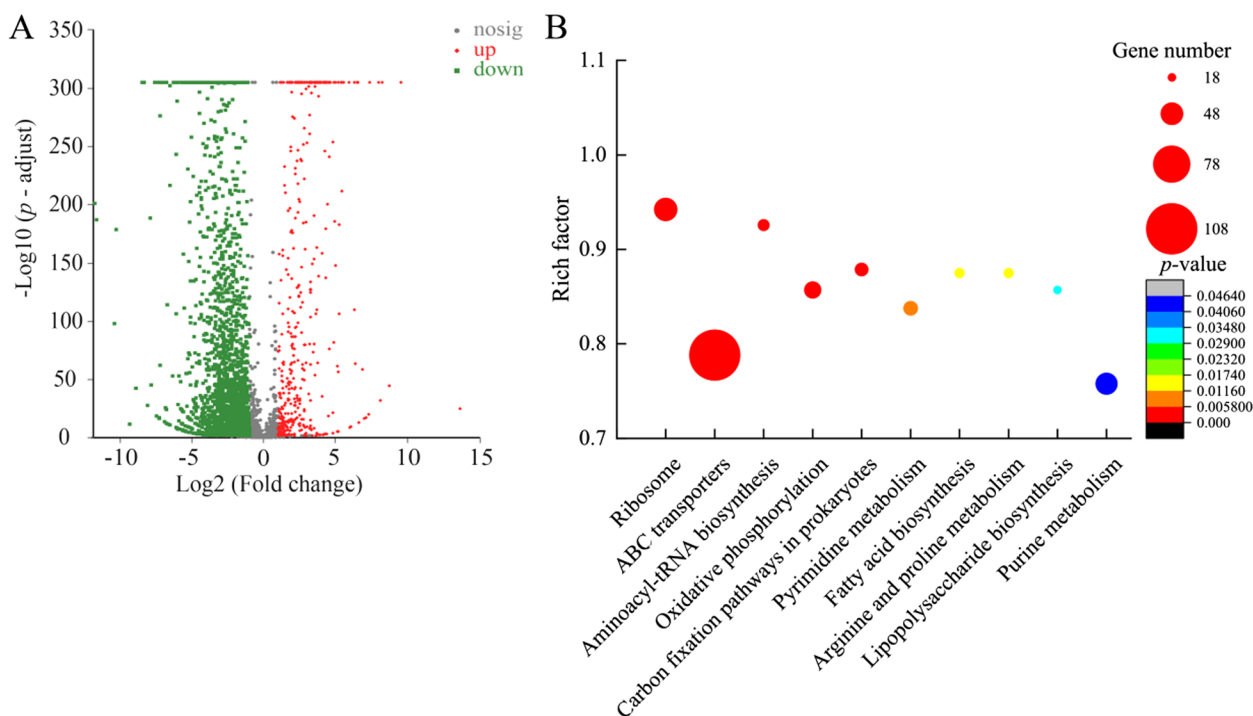

Fig. 7 The Volcano plot of differential gene expression (**A**), and the major changed metabolic pathways (**B**) in *V. parahaemolyticus* ATCC17802 under the hypoxic condition

Xu *et al. Annals of Microbiology*   (2024) 74:20

Page 16 of 23

the pyrimidine metabolism, the DEG encoding a 5' deoxynucleotidase (*Vp_17802_04570*, 4.317–fold) was highly up-regulated in *V. parahaemolyticus* ATCC17802 ($p < 0.05$). This enzyme is involved in the metabolism of cladribine (2CdA), by mediating phosphorolysis (deactivation) of 2CdA to prevent its accumulation in the cell, which leads to cell death (Carlini et al. 2022).

The same cases as *V. parahaemolyticus* B1-21, and N2-5 isolates, all the DEGs ($n = 49$) in the ribosome were highly down-regulated (0.033–fold to 0.243–fold) in *V. parahaemolyticus* ATCC17802 under the hypoxic condition ($p < 0.05$). Similar to *V. parahaemolyticus* B8-26, B1-21, and N2-5 isolates, almost all DEGs (105/108) in the ABC transporters were also significantly repressed (0.001–fold to 0.479–fold) in *V. parahaemolyticus* ATCC17802 ($p < 0.05$). Like *V. parahaemolyticus* B8-26, N2-5, and L7-40 isolates, most DEGs (19/21) in the carbon fixation pathways in prokaryotes were significantly inhibited (0.049–fold to 0.359–fold) in *V. parahaemolyticus* ATCC17802 ($p < 0.05$). In addition, like *V. parahaemolyticus* B8-26, all DEGs ($n = 25$) in the aminoacyl-tRNA biosynthesis were significantly repressed (0.100–fold to 0.477–fold) in *V. parahaemolyticus* ATCC17802 as well ($p < 0.05$).

Taken, the comparative transcriptome analysis revealed ten significantly changed metabolic pathways in *V. parahaemolyticus* ATCC17802 under the hypoxic condition. Although some of the altered pathways were also observed in *V. parahaemolyticus* B8-26, B1-21, N2-5, and L7-40 isolates, however, wherein more repressed DEGs were elicited in *V. parahaemolyticus* ATCC1780 by the condition, consistent with the phenotypes of this isolate in the above results. In particular, compared to the other four *V. parahaemolyticus* isolates, *V. parahaemolyticus* ATCC17802 also down-regulated some metabolic pathways, including the pyrimidine metabolism, fatty acid biosynthesis, lipopolysaccharide biosynthesis, purine metabolism, as well as arginine and proline metabolism to survival under the hypoxic condition.

Additionally, to confirm the transcriptome data, thirty representative DEGs were analyzed by the RT-qPCR assay, and the resulting data were generally correlated with those by the transcriptome analysis (Table S12).

Possible molecular mechanisms of *V. parahaemolyticus* in response to the hypoxic condition

The transcriptome-wide analyses revealed a number of DEGs involved in multiple pathways of biosynthesis, degradation, salvage, interconversion, and transport of the compounds in *V. parahaemolyticus* B8-26, B1-21, N2-5, L7-40 and ATCC17802 isolates of aquatic animal and human clinical origins, suggesting a complex molecular regulation network in the bacterium in response to the hypoxic condition (Fig. S7, Table S13).

Given that the *V. parahaemolyticus* isolates, being from different origins, harbored different genome features, it was reasonable that the hypoxic condition triggered different transcriptomic profiles among the isolates. The transcriptome data, coupled with the phenotype results in this study, demonstrated that compared to the other isolates, *V. parahaemolyticus* ATCC17802 down-regulated and/or shut down all the ten changed metabolic pathways to reduce cell viability and maintain cell structure integrated under the hypoxic condition. These results provided a novel mechanism for the persistence of the toxic strain in the environment and in the host.

On the other hand, same identical metabolic pathways were elicited in the *V. parahaemolyticus* isolates by the hypoxic condition, e.g., the inhibited ribosome in *V. parahaemolyticus* B1-21, N2-5, and ATCC17802 isolates; the repressed aminoacyl-tRNA biosynthesis in *V. parahaemolyticus* B8-26, and ATCC17802 isolates; and the repressed oxidative phosphorylation in *V. parahaemolyticus* N2-5, L7-40, and ATCC17802 isolates.

Overall, *V. parahaemolyticus* developed multiple molecular strategies to efficiently mitigate the cell damage and/or cytotoxicity caused by the hypoxia: (1) down-regulated the oxidative phosphorylation, carbon fixation pathways, citrate cycle, pyruvate metabolism, and propionate metabolism to balance the redox state of the cell and the energy conversion; (2) down-regulated the fatty acid biosynthesis, and lipopolysaccharide biosynthesis to inhibit the cell wall synthesis, thereby the cell proliferation; (3) decreased amino acid transport, aminoacyl-tRNA biosynthesis, and protein production to retard the cell growth, thus prolonging the growth cycle and maintaining the cell structure integrated; and (4) conversely, enhanced the expression of condition-related proteins (such as GapA), structurally stabilizing factors (such as arginine), and efflux RND transporters to reduce the cell damage for growth under the unfavorable hypoxic condition.

Serotypes of the *V. parahaemolyticus* isolates

The BLAST analysis of the antigen gene loci reveled that the *V. parahaemolyticus* B8-26 and B1-21 genomes contained the O antigen loci *wvaG*/*wvcA*, and specific loci *VP6* and *VP202* for K34 and K23 polymorphic sites, respectively, indicating that the serotypes of *V. parahaemolyticus* B8-26, and B1-21 isolates were O1:K34, and O5:K23, respectively. Similarly, *V. parahaemolyticus* N2-5, and L7-40 genomes carried O antigen loci *orf16*/*wzy* and *wvaH*, indicating that the serotypes of *V. parahaemolyticus* N2-5, and L7-40 isolates were O4/O11:K4, and O9:KUT, respectively. Additionally, *V.*

Xu *et al. Annals of Microbiology*   (2024) 74:20

Page 17 of 23

parahaemolyticus ATCC17802 carried O antigen loci *gmd*, and specific loci *VP199* for K1 polymorphic sites, and its serotype was O1:K1 (Bian et al. 2020).

Phylogenetic relatedness of the *V. parahaemolyticus* isolates

To address the phylogenetic relatedness of the *V. parahaemolyticus* isolates, we constructed a phylogenetic tree based on a total of 1,921 homologous amino acid sequences identified from the seventy-eight *V. parahaemolyticus* genomes, seventy-four of which were derived from the GenBank database (Table S1). This analysis revealed ten different phylogenetic groups, designated as Groups 1–10 (Fig. 8).

V. parahaemolyticus B8-26 (serotype: O1:K34; GenBank accession number: JAODUR000000000) was classified into Group 8, showing the closest evolutionary distance with *V. parahaemolyticus* XMM117 (serotype: O3:K6; GenBank accession number: NZ_CP064037.1), which was isolated from the environment in 2019 in China.

V. parahaemolyticus L7-40 (serotype: O9:KUT; GenBank accession number JAODVU000000000) fell into Group 4, together with *V. parahaemolyticus* FDAAR-GOS-667 (serotype: O5:K33/K55; GenBank accession number: NZ_CP044062.1), which was isolated from Homo sapiens in USA (collection time unknown).

V. parahaemolyticus B1-21 (serotype: O5:K23; GenBank accession number: JAOPTY000000000), and *V. parahaemolyticus* N2-5 (serotype: O4/O11:K4; GenBank accession number: JAODVT000000000) were classified into single evolutionary branches Groups 3, and 9, respectively, indicating that these two isolates have unique genome features.

In addition, the *V. parahaemolyticus* strains that can cause gastroenteritis in humans were classified into Groups 1, 2, 5, 6, 7, and 8, e.g., *V. parahaemolyticus* ATCC17802 (serotype: O1:K1; GenBank accession number: NZ_CP014046.1) in Group 2; *V. parahaemolyticus* 64 (serotype: O1:KUT; GenBank accession number: NZ_CP074415.1) isolated from Penaeus in Group 1; and *V. parahaemolyticus* XMM117 (serotype: O3:K6; GenBank accession number: NZ_CP064037.1) isolated from the environment in Group 8.

Taken, these results demonstrated the diversity of *V. parahaemolyticus* genomes of the environmental and clinical origins.

Discussion

Infectious diseases caused by pathogenic bacteria continue to be a global concern for public health, which results in millions of deaths worldwide each year (Bueno et al. 2020). The sea foodborne illness caused by *V. parahaemolyticus* has shown a significant upward trend in
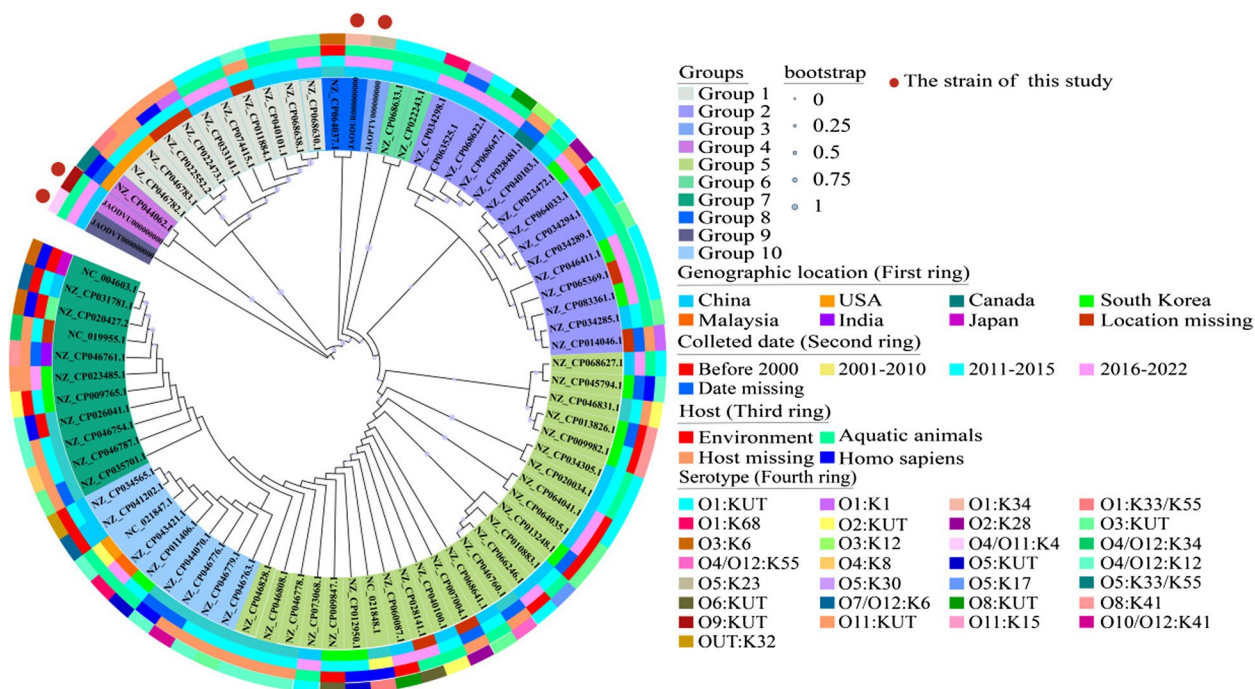

Fig. 8 The phylogenetic tree showing the relationship of the seventy-eight *V. parahaemolyticus* genomes. Draft genome sequences of the *V. parahaemolyticus* isolates determined in this study were marked with red dots in the tree

Xu *et al. Annals of Microbiology*   (2024) 74:20

Page 18 of 23

recent years (Zhai et al. 2021). Climate change is driving ocean oxygen declines (Jaccard and Galbraith 2012). On the other hand, the low oxygen level in the human gastrointestinal tract also challenges the survival and infection of *V. parahaemolyticus*. Thus, in the present study, we for the first time investigated how *V. parahaemolyticus* isolates of aquatic animal and human clinical origins response to the hypoxic condition.

V. parahaemolyticus B8-26, B1-21, N2-5, and L7-40 strains were isolated from aquatic animals *S. strictus, C. aurea, O. oratoria*, and *C. idellus*, respectively (Su and Chen 2020). Multiple antibiotic and heavy metal resistance profiles were derived from the four *V. parahaemolyticus* isolates, suggested possible antibiotic and heavy metal exposure or pollution sources in the aquaculture environments (Su and Chen 2020; Xu et al. 2022a). Moreover, we observed that these isolates grew optimally in the TSB medium with 3% NaCl and pH 8.5 at 37 ℃, consistent with the previous report (Xu et al. 2022a).

V. cholerae is a member of the *Vibrio* genus and can cause pandemic cholerae in humans (Ramamurthy et al. 2020). *V. cholerae* was able to generate energy and maintain its physiological functions in the absence of oxygen using alternative electron acceptors (AEAs) (Bueno et al. 2020). In this study, we determined growth curves of the *V. parahaemolyticus* isolates in the TSB equalibrated with different oxygen concentrations (21–5% O_2) at 37 ℃. Unlike *V. cholerae,* our data showed that the lower oxygen concentrations (5–10%) greatly inhibited the growth of the tested isolates. However, no significant difference in the growth was observed between 5% O_2 and 10% O_2, suggesting that 10% O_2 was the cut-off point for the growth of *V. parahaemolyticus* at the low oxygen concentrations. Additionally, we observed that oxygen concentrations in air within the culture tubes fluctuated down by 0–1% within 24 h, and by 0–2% from 24 to 48 h, indicating the stable hypoxic condition maintained in our culture system.

Biofilm is critical for *V. parahaemolyticus* persistence in aquatic environments and pathogenicity in the host (Yildiz and Visick 2009). In this study, the results showed that the biofilm biomass generated by all the tested *V. parahaemolyticus* isolates under the 10% O_2 condition was significantly increased at the development and maturation stages (0–36 h) ($p < 0.05$), as compared to those under the normal 21% O_2 condition. It has been reported that biofilm formation of *P. aeruginosa, S. aureus*, and *E. coli* induced the production of hypoxia-related enzymes (Crespo et al.2016; Jo et al. 2017; Létoffé et al. 2017). Our results, coupled with these previous studies, suggested that biofilm formation was likely beneficial to the pathogenic bacteria to survival under lower oxygen niches.

Unexpectedly, we found that the pathogenic *V. parahaemolyticus* ATCC17802 was capable of maintaining more rod-shaped cells with no surface shrinkage than the other tested isolates, demonstrating that *V. parahaemolyticus* ATCC17802 was the most tolerant to the hypoxia. This may attribute to its survial in the host gastrointestinal tract with low oxygen level.

Draft genomes of the four *V. parahaemolyticus* isolates from aquatic animals were determined (4.91–5.35 Mb), with no plasmid sequenced. Clean single peaks with a typical Poisson distribution in the frequency of observed unique 17-mers within the sequencing data indicated less repetitive DNA in the genomes, consistent with the fewer ISs identified in the *V. parahaemolyticus* genomes. Among the 4,458–4,924 predicted genes, 735 to 1,046 encoded unknown proteins. A large number of unknown genes have also been reported in seven *V. parahaemolyticus* genomes of aquatic animal origins in the previous report (Xu et al. 2022a).

V. parahaemolyticus B8-26, B1-21, N2-5, and L7-40 genomes also carried MGEs. Only one identified IS (*V. parahaemolyticus* L7-40 genome in IS001) was present at the end of the scaffold 84 and scaffold 86 (Table S14), suggesting that the assembled genomes did not result in the loss of identified MGEs (except for this IS001). Of note, the *V. parahaemolyticus* B1-21 genome had the maximum numbers of INs ($n=11$) and prophage gene clusters ($n=2$), while the *V. parahaemolyticus* N2-5, and B8-26 genomes carried the maximum numbers of GIs ($n=14$), and ISs ($n=4$), respectively. The MGEs, such as GIs ($n=5$–9), prophage gene clusters ($n=0$–2), INs ($n=1$–11), and ISs ($n=0$–3) have also been reported in *V. parahaemolyticus* isolates from six species of aquatic animals (Xu et al. 2022a). Several MGEs were found in *V. parahaemolyticus* ATCC17802 (Yang et al. 2015) as well, including GIs ($n=2$), and INs ($n=7$). These results in this study, coupled with the previous reports (Xu et al. 2022a; Yu et al. 2022; Yang et al. 2015), indicated possible HGT via the MGEs during the *V. parahaemolyticus* evolution. The MGEs, with diverse gene functions identified in this study, can promote ecological niche adaptation, alter gene availability within microbial communities, and drive the bacterial evolution (Tuttle et al. 2022). CRISPR-Cas systems provide adaptive immunity for bacteria to resist foreign DNA invasion (Zaayman et al. 2022). In this study, CRISPR-Cas gene clusters (75–189 bp) were found in the *V. parahaemolyticus* B1-21 ($n=1$), N2-5 ($n=1$), L7-40 ($n=3$), and ATCC17802 ($n=4$) genomes, but none of which carried Cas protein-coding gene, suggesting partial or inactive CRISPR-Cas systems in these *V. parahaemolyticus* isolates (Fig. S8).

Most types of *Vibrio* species have an extensive reservoir of virulence genes (Abdelaziz Gobarah et al. 2022). In this study, although no toxic *tdh* and *trh* genes (Ceccarelli et al. 2013) were found, virulence-related genes (42–45)

Xu *et al. Annals of Microbiology*   (2024) 74:20

Page 19 of 23

were identified in the four *V. parahaemolyticus* genomes of aquatic animal origins, e.g., *ilpA*, *MAM7*, *exsA*, flagella, *Al-2*, *VpadF*, and T3SS1-related genes. T3SSs are important determinants in *V. parahaemolyticus* pathogenicity (Raval et al. 2021). In our previous study, we also found a number of virulence-related genes (e.g., *impI*, *vgrG*, *fliC-DEFG*, *flrBC*, *yscOPQRST*, and *T6SS*-related genes) in *V. parahaemolyticus* strains recovered from six species of aquatic animals (Xu et al. 2022a). These results suggested possible health risks in consuming these aquatic animals.

In this study, a few antibiotic resistance-related genes, which are responsible for the fluoroquinolone (*crp*), TET (*Tet* (*35*)), and beta-lactam ($bla_{CARB-18}$) resistance, were identified in the *V. parahaemolyticus* genomes, consistent with the observed phenotypes. Moreover, several heavy metal tolerance-related genes (e.g., *cusARS*, *dsbABC*, *smtA*, *zntA*) were found in these *V. parahaemolyticus* isolates as well. For example, the *smtA* and *zntA* genes, which are involved in bacterial tolerance to Zn, as well as Hg and Zn, respectively (Chen et al. 2021; Lee et al. 2001; Pal et al. 2014), were present in the *V. parahaemolyticus* B8-26, B1-21, L7-40, and ATCC17802 genomes. *V. parahaemolyticus* B8-26 also carried the *cusARS* and *dsbABC* gene clusters, which are involved in bacterial tolerance to Cu, as well as Cd, Zn, Hg and Cu, respectively. The antibiotic resistance-related genes (such as *acrB*, *catB*, *hns*, *qnr*, *soxR*), and heavy metal tolerance-related genes (e.g., *copA*, *cusA*, *cusR*, *cusS*, *zntA*) have also been reported in the *V. parahaemolyticus* genomes derived from six species of aquatic animals (Xu et al. 2022a).

The transcriptomic analyses revealed distinct response strategies to hypoxia by *Vibrio parahaemolyticus* isolates of clinical and aquatic animal origins. Different degrees of impact on the growth of *V. parahaemolyticus* isolates were observed, which were triggered by the hypoxic condition. For instance, all DEGs were significantly down-regulated in the PG biosynthesis, as well as ubiquinone and other terpenoid-quinone biosynthesis in *V. parahaemolyticus* B8-26 ($p < 0.05$). In response to the hypoxic condition, *V. parahaemolyticus* L7-40 inhibited the glyoxylate and dicarboxylate metabolism, but up-regulated the glycolysis/gluconeogenesis, and changed the nitrogen metabolism, and the arginine biosynthesis ($p < 0.05$). The transcriptome data, coupled with the phenotype results in this study, demonstrated that *V. parahaemolyticus* ATCC17802 was the most tolerant to the hypoxia among the isolates. This isolate down-regulated and/or shut down all the ten changed metabolic pathways to reduce cell viability and maintain cell structure under the hypoxic condition. In particular, the pyrimidine metabolism, fatty acid biosynthesis, LPS biosynthesis, purine metabolism, as well as arginine and proline metabolism were all repressed in *V. parahaemolyticus* ATCC17802.

Fatty acids are essential for biosynthesis of phospholipids and also provide ATP, signaling molecules, and NADPH through *β*-oxidation (Chen et al. 2022). For example, the DEG encoding a *β*-ketoacyl-ACP synthase (*Vp_17802_11840*) in the fatty acid biosynthesis was significantly down-regulated (0.200–fold) in *V. parahaemolyticus* ATCC17802 ($p < 0.05$), which play a vital role in cell wall synthesis, biofilm formation and also pathogenesis (Hu et al. 2020). These results provided a novel mechanism for the persistence of the toxic strain in the environment and in the host.

Additionally, some metabolic pathways were altered in the all *V. parahaemolyticus* isolates under the hypoxic condition, e.g., the inhibited ribosome in *V. parahaemolyticus* B1-21, N2-5, and ATCC17802 isolates; the repressed aminoacyl-tRNA biosynthesis in *V. parahaemolyticus* B8-26, and ATCC17802 isolates; the inhibited oxidative phosphorylation in *V. parahaemolyticus* N2-5, L7-40, and ATCC17802 isolates; and the suppressed citrate cycle in *V. parahaemolyticus* B8-26, N2-5, and L7-40 isolates ($p < 0.05$). For instance, the DEGs encoding the fumarate reductase subunits FrdCD, which is involved in maintaining redox balance through regeneration of reduced cofactors during oxygen deficiency conditions (Sędzielewska et al. 2012), were significantly repressed in *V. parahaemolyticus* B8-26 (*Vp_B8-26_15850*, 0.107–fold; *Vp_B8-26_15855*, 0.087–fold), *V. parahaemolyticus* B1-21 (*Vp_B1-21_15850*, 0.406–fold; *Vp_B1-21_15855*, 0.341–fold), *V. parahaemolyticus* N2-5 (*Vp_N2-5_15850*, 0.149–fold; *Vp_N2-5_15855*, 0.230–fold), *V. parahaemolyticus* ATCC17802 (*Vp_17802_15850*, 0.248–fold; *Vp_17802_15855*, 0.113–fold), and *V. parahaemolyticus* L7-40 (FrdD, *Vp_L7-40_15855*, 0.417–fold). Most of the DEGs in the oxidative phosphorylation were also significantly repressed in *V. parahaemolyticus* N2-5, L7-40, and ATCC17802 isolates, which possibly provided indirect evidence for the hypoxic condition maintained in our culture system. The oxidative phosphorylation is the last metabolic pathway of cellular respiration, for the production of ATP, the "energy currency" to sustain life (Wilson 2017).

Taken, *V. parahaemolyticus* developed multiple molecular strategies to balance the redox state of the cell and the energy conversion, to inhibit the cell wall synthesis, thereby the cell proliferation, to retard the cell growth, thus prolonging the growth cycle and maintaining the cell structure integrated, to enhance the expression of stress-related proteins, structurally stabilizing factors, and efflux RND transporters, in order to efficiently mitigate the cell damage and/or cytotoxicity caused by the hypoxia.

Conclusions

In this study, we investigated, for the first time, the growth of *V. parahaemolyticus* B8-26, B1-21, N2-5, L7-40, and ATCC17802 isolates under the hypoxic

Xu *et al. Annals of Microbiology*   (2024) 74:20

Page 20 of 23

condition. The former four were isolated from *S. stritus, C. aurea, O. oratoria,* and *C. idellus*, respectively, while *V. parahaemolyticus* ATCC17802 was of human clinical origin. These isolates harbored multiple antibiotic and heavy metal resistance phenotypes, and grew optimally in the TSB (3% NaCl, pH 8.5) at 37 °C.

V. parahaemolyticus B8-26, B1-21, N2-5, L7-40, and ATCC17802 isolates had an oxygen concentration-dependent growth mode, and the 10% O_2 condition strongly inhibited the growth of the isolates, when incubated in TSB medium at 37 °C. Unexpectedly, in marked contrast to the normal 21% O_2 condition, the *V. parahaemolyticus* isolates enhanced biofilm formation under the hypoxic condition for 24 h.

Draft genome sequences of *V. parahaemolyticus* B8-26 (serotype: O1:K34), B1-21 (serotype: O5:K23), N2-5 (serotype: O4/O11:K4), and L7-40 (serotype: O9: KUT) were determined (4,913,675–5,353,490 bp). Comparative genomic analysis revealed unknown function genes (19.32–23.13%), and MGEs ($n = 12$–29) in the *V. parahaemolyticus* genomes. Moreover, *V. parahaemolyticus* B1-21, and N2-5 had unique genome features, classified into single branches in the phylogenetic tree.

Genome-wide gene expression changes triggered by the hypoxic condition were further examined. Comparative transcriptomic analysis unveiled multiple significantly changed metabolic pathways in the isolates under the 10% O_2 condition for 24 h. *V. parahaemolyticus* developed multiple molecular strategies to efficiently mitigate the cell damage and/or cytotoxicity caused by the hypoxia.

In addition, *V. parahaemolyticus* ATCC17802 (serotype: O1:K1) of the clinical origin was the most tolerant to the hypoxia among the test isolates, and down-regulated and/or shut down ten metabolic pathways to reduce cell viability and prolong growth under the stress.

Overall, the results of this study fill prior gaps in *V. parahaemolyticus* response to the hypoxic condition, and provide a novel mechanism for the toxic *V. parahaemolyticus* strain to persist in the environment and in the host.

Supplementary Information

The online version contains supplementary material available at https://doi.org/10.1186/s13213-024-01769-4.

Supplementary Material 1:b Fig. S1. The growth of the *V. parahaemolyticus* isolates in the TSB (pH 8.5) under different concentrations of NaCl at 37 °C. A–E: *V. parahaemolyticus* B8-26, B1-21, N2-5, L7-40, and ATCC17802, respectively. Fig. S2. The growth of the *V. parahaemolyticus* isolates in the TSB (3% NaCl) under different pH conditions at 37 °C. A–E: *V. parahaemolyticus* B8-26, B1-21, N2-5, L7-40, and ATCC17802, respectively. Fig. S3. The growth of the *V. parahaemolyticus* isolates in the TSB (pH 8.5, 3% NaCl) at 25 °C and 37 °C. A–E: *V. parahaemolyticus* B8-26, B1-21, N2-5, L7-40, and ATCC17802, respectively. Fig. S4. The genome circle maps of the four *V.*

parahaemolyticus isolates of aquatic animal origins. (A–B): The larger and smaller chromosomes of the four *V. parahaemolyticus* isolates, respectively. Circles from the inwards to outside represent the GC content (outward and inward values indicate above and below average, respectively); GC-skew (purple and green values are more and less than zero, respectively); the reference genome of *V. parahaemolyticus* RIMD 2210633 (GenBank accession no. NC_004603.1); *V. parahaemolyticus* B8-26, B1-21, N2-5, and L7-40 genomes, respectively; and CDSs on the positive and negative chains (inward and outward parts), respectively. Fig. S5. The structure diagram of the INs identified in the *V. parahaemolyticus* genomes. The complete INs and incomplete gene cassettes identified in *V. parahaemolyticus* B8-26, B1-21, N2-5, L7-40, and ATCC17802 genomes are shown, with the predicted *attc* sites and ORFs. Fig. S6. COG annotation classification statistics of the *V. parahaemolyticus* genomes. Fig. S7. Possible molecular strategies developed by *V. parahaemolyticus* under the hypoxia. SD: sugars and derivatives; FP: flavoprotein; F: ferritin; SA: succinic acid; OA: oxaloacetate; AC: acetyl coenzyme; P: pyruvate; MG: methylglyoxal; FAS: fatty acid synthase; C: coenzyme; ACP: acyl carrier protein; FAP: flagellar assembly protein; G: glutamine; S: serine; L: leucine; GapA: stress-related proteins; A: arginine; and RND: efflux RND transporters. Fig. S8. The structural features of CRISPRs identified in the *V. parahaemolyticus* genomes. The repeat sequences were shown by the rectangle in different colors and the spacer regions were represented by rhombuses in different colors.

Supplementary Material 2: Table S1. The information of the 78 V. *parahaemolyticus* genomes analyzed in the phylogenetic tree. Table S2. The oligonucleotide primers designed and used in the RT-qPCR assay. Table S3. The identified GIs in the *V. parahaemolyticus* genomes. Table S4. The identified prophages in the *V. parahaemolyticus* genomes. Table S5. The identified INs in the *V. parahaemolyticus* genomes. Table S6. The identified ISs in the *V. parahaemolyticus* genomes. Table S7. The major changed metabolic pathways in *V. parahaemolyticus* B8-26 under the hypoxic condition. Table S8. The major changed metabolic pathways in *V. parahaemolyticus* B1-21 under the hypoxic condition. Table S9. The major changed metabolic pathways in *V. parahaemolyticus* N2-5 under the hypoxic condition. Table S10. The major changed metabolic pathways in *V. parahaemolyticus* L7-40 under the hypoxic condition. Table S11. The major changed metabolic pathways in *V. parahaemolyticus* ATCC17802 under the hypoxic condition. Table S12. The relative expression of representative DEGs in the *V. parahaemolyticus* isolates by the RT-PCR assay. Table S13. Comparison of the major altered metabolic pathways in the five *V. parahaemolyticus* isolates under the hypoxic stress. Table S14. The identified repeats at the end of scaffolds of the *V. parahaemolyticus* genomes.

Authors' Contributions
H.X.: the major investigation, data curation, and writing-original draft preparation; B.Z.: the hypoxic condition experiments; P.Y.: writing-review and editing; M.S.: the transcriptome data analyses; L.X.: supervision, discussion, and writing-review and editing; L.C.: funding acquisition, conceptualization, and writing-review and editing. All authors have read and agreed to the published version of the manuscript.

Availability of data and materials
Draft genome sequences of the four *V. parahaemolyticus* isolates of aquatic animal origins have been deposited in the GenBank database under the accession numbers: JAODUR000000000, JAOPTY000000000, JAODVT000000000, and JAODVU000000000. A complete list of the DEGs is available in the NCBI SRA database (https://www.ncbi.nlm.nih.gov/) under the accession number PRJNA906699 and PRJNA767551.

Xu *et al. Annals of Microbiology* (2024) 74:20

Page 21 of 23

Declarations

Ethics approval and consent to participate
This article does not contain any studies with human participants or animals performed by any of the authors.

Consent for publication
Not applicable.

Competing interests
The authors declare that they have no competing interests.

Author details
[1]Key Laboratory of Quality and Safety Risk Assessment for Aquatic Products On Storage and Preservation (Shanghai), Ministry of Agriculture and Rural Affairs of the People's Republic of China, College of Food Science and Technology, Shanghai Ocean University, Shanghai 201306, China. [2]Shanghai-MOST Key Laboratory of Health and Disease Genomics, Institute for Genome and Bio-Informatics, Shanghai Institute for Biomedical and Pharmaceutical Technologies, Fudan University, Shanghai, China.

References

Abdelaziz Gobarah DE, Helmy SM, Mahfouz NB, Fahmy HA, Abou Zeid M (2022) Virulence genes and antibiotic resistance profile of *Vibrio* species isolated from fish in egypt. Vet Res Forum. 13:315–321. https://doi.org/10.30466/vrf.2021.520767.3117

Aggarwal SD, Lloyd AJ, Yerneni SS, Narciso AR, Shepherd J, Roper DI (2021) A molecular link between cell wall biosynthesis, translation fidelity, and stringent response in *Streptococcus pneumoniae*. Proc Natl Acad Sci USA 118:e2018089118. https://doi.org/10.1073/pnas.2018089118

Ali N, Lin Y, Jiang L, Ali I, Ahmed I, Akhtar K (2022) Biochar and manure applications differentially altered the class 1 integrons, antimicrobial resistance, and gene cassettes diversity in paddy soils. Front Microbiol 13:943880. https://doi.org/10.3389/fmicb.2022.943880

Alqahtani FY, Aleanizy FS, El Tahir E, Alkahtani HM, AlQuadeib BT (2019) Paclitaxel. Chapter Three - Paclitaxel. Profiles of Drug Substances, Excipients and Related Methodology 44:205–238. https://doi.org/10.1016/bs.podrm.2018.11.001

Bian S, Zeng W, Li Q, Li Y, Wong NK, Jiang M (2020) Genetic structure, function, and evolution of capsule biosynthesis loci in *Vibrio parahaemolyticus*. Front Microbiol 11:546150. https://doi.org/10.3389/fmicb.2020.546150

Bueno E, Sit B, Waldor MK, Cava F (2018) Anaerobic nitrate reduction divergently governs population expansion of the enteropathogen *Vibrio cholerae*. Nat Microbiol 3:1346–1353. https://doi.org/10.1038/s41564-018-0253-0

Bueno E, Pinedo V, Cava F (2020) Adaptation of *Vibrio cholerae* to hypoxic environments. Front Microbiol 11:739. https://doi.org/10.3389/fmicb.2020.00739

Calisto F, Pereira MM (2021) The Ion-translocating NrfD-Like subunit of energy-transducing membrane complexes. Front Chem 9:663706. https://doi.org/10.3389/fchem.2021.663706

Carlini F, Ivaldi F, Gualandi F, Boschert U, Centonze D, Matarese G (2022) Different susceptibility of T and B cells to cladribine depends on their levels of deoxycytidine kinase activity linked to activation status. J Neuroimmune Pharmacol 17:195–205. https://doi.org/10.1007/s11481-021-09994-3

Ceccarelli D, Hasan NA, Anwar Huq A, Colwell RR, R R, (2013) Distribution and dynamics of epidemic and pandemic *Vibrio parahaemolyticus* virulence factors. Front Cell Infect Microbiol 3:97. https://doi.org/10.3389/fcimb.2013.00097

Chen CC, Gong GC, Shiah FK (2007) Hypoxia in the east China sea: one of the largest coastal low-oxygen areas in the world. Mar Environ Res 64:399–408. https://doi.org/10.1016/j.marenvres.2007.01.007

Chen H, Yang Z, Sun Y, Yin S, Tang M, Zhang F (2022) Targeting the key enzymes of abnormal fatty acid β-oxidation as a potential strategy for tumor therapy. Front Biosci 27:95. https://doi.org/10.31083/j.fbl2703095

Chen M, Wang L, Zheng X, Cohen M, Li X (2021) Cross-Kingdom comparative transcriptomics reveals conserved genetic modules in response to cadmium stress. mSystems 6:e01189–01121.https://doi.org/10.1128/mSystems.01189-21

Crespo A, Pedraz L, Astola J, Torrents E (2016) Pseudomonas aeruginosa exhibits deficient biofilm formation in the absence of class II and III ribonucleotide reductases due to hindered anaerobic growth. Front Microbiol 7:688. https://doi.org/10.3389/fmicb.2016.00688

Damale MG, Patil R, Ansari SA, Alkahtani HM, Ahmed S, Nur EAM (2022) Insilico structure based drug design approach to find potential hits in ventilator-associated pneumonia caused by *Pseudomonas aeruginosa*. Comput Biol Med 146:105597. https://doi.org/10.1016/j.compbiomed.2022.105597

Emms D, Kelly S (2019) OrthoFinder: phylogenetic orthology inference for comparative genomics. Genome Biol 20:238. https://doi.org/10.1186/s13059-019-1832-y

Fanelli GN, Scarpitta R, Cinacchi P, Fuochi B, Szumera-Ciećkiewicz A, De Ieso K (2021) Immunohistochemistry for thymidine kinase-1 (TK1): a potential tool for the prognostic stratification of breast cancer patients. J Clin Med 10:5416. https://doi.org/10.3390/jcm10225416

Fujino T, Okuno Y, Nakada D, Aoyama A, Fukai K, Mukai T, Ueho T (1953) On the bacteriological examination of shirasu-food poisoning. Med J Osaka Univ 4:299–304

Gao K, Helbling EW, Häder DP, Hutchins DA (2012) Responses of marine primary producers to interactions between ocean acidification, solar radiation, and warming. Mar Ecol Prog Ser 470:167–189. https://doi.org/10.3354/meps10043

Garavito MF, Narváez-Ortiz HY, Zimmermann BH (2015) Pyrimidine metabolism: dynamic and versatile pathways in pathogens and cellular development. J Genet Genomics. 42:195–205. https://doi.org/10.1016/j.jgg.2015.04.004

Ghazali AK, Eng SA, Khoo JS, Teoh S, Hoh CC, Nathan S (2021) Whole-genome comparative analysis of malaysian *pseudomallei* clinical isolates. Microb Genom 7:000527. https://doi.org/10.1099/mgen.0.000527

Goudarzi A (2019) The recent insights into the function of ACAT1: a possible anti-cancer therapeutic target. Life Sci 232:116592. https://doi.org/10.1016/j.lfs.2019.116592

Gu D, Zhang Y, Wang Q, Zhou X (2020) S-nitrosylation-mediated activation of a histidine kinase represses the type 3 secretion system and promotes virulence of an enteric pathogen. Nat Commun 11:5777. https://doi.org/10.1038/s41467-020-19506-1

Günenc AN, Graf B, Stark H, Chari A (2022) Fatty acid synthase: structure, function, and regulation. Subcell Biochem 99:1–33. https://doi.org/10.1007/978-3-031-00793-4_1

Heidelberg JF, Eisen JA, Nelson WC, Clayton RA, Gwinn ML, Dodson RJ (2000) DNA sequence of both chromosomes of the cholera pathogen *Vibrio cholerae*. Nature 406:477–483. https://doi.org/10.1038/35020000

Hosseini N, Pourhajibagher M, Chiniforush N, Hosseinkhan N, Rezaie P, Bahador A (2019) Modulation of toxin-antitoxin system Rnl AB type II in phage-resistant gammaproteobacteria surviving photodynamic treatment. J Lasers Med Sci. 10:21–28. https://doi.org/10.15171/jlms.2019.03

Hu F, Huang Z, Zheng S, Wu Q, Chen Y, Lin H (2020) Structural and biochemical characterization of inorganic pyrophosphatase from homo sapiens. Biochem Biophys Res Commun 533:1115–1121. https://doi.org/10.1016/j.bbrc.2020.09.139

Jaccard SL, Galbraith ED (2012) Large climate-driven changes of oceanic oxygen concentrations during the last deglaciation. Nat Geosci 5:151–156. https://doi.org/10.1038/ngeo1352

Jeong HH (2021) Recent developments in bacterial chemotaxis analysis based on the microfluidic system. SLAS Technol 26:159–164. https://doi.org/10.1177/2472630320969146

Jin J, Zhou Y, Zhang Z, Wang H, Hou W, Wang H (2021) Characteristics of antimicrobial-resistant *Vibrio parahaemolyticus* strains and identification of related antimicrobial resistance gene mutations. Foodborne Pathog Dis 18:873–879. https://doi.org/10.1089/fpd.2020.2911

Jo J, Cortez KL, Cornell WC, Price-Whelan A, Dietrich LE (2017) An orphan cbb$_3$-type cytochrome oxidase subunit supports *Pseudomonas* aeruginosa biofilm growth and virulence. Elife 6:e30205. https://doi.org/10.7554/eLife.30205

Karan S, Choudhury D, Dixit A (2021) Immunogenic characterization and protective efficacy of recombinant CsgA, major subunit of curli fibers,

Xu *et al. Annals of Microbiology*   (2024) 74:20

Page 22 of 23

against *Vibrio parahaemolyticus*. Appl Microbiol Biotechnol 105:599–616. https://doi.org/10.1007/s00253-020-11038-4

Khan F, Tabassum N, Anand R, Kim YM (2020) Motility of *Vibrio* spp.: regulation and controlling strategies. Appl Microbiol Biotechnol 104:8187–8208. https://doi.org/10.1007/s00253-020-10794-7

Kierans SJ, Taylor CT (2021) Regulation of glycolysis by the hypoxia-inducible factor (HIF): implications for cellular physiology. J Physiol 599:23–37. https://doi.org/10.1113/jp280572

Kies PJ, Hammer ND (2022) A resourceful race: bacterial scavenging of host sulfur metabolism during colonization. Infect Immun 90:e0057921. https://doi.org/10.1128/iai.00579-21

Kim S, Kim CM, Son YJ, Choi JY, Siegenthaler RK, Lee Y (2018) Molecular basis of maintaining an oxidizing environment under anaerobiosis by soluble fumarate reductase. Nat Commun 9:4867. https://doi.org/10.1038/s41467-018-07285-9

Komar J, Alvira S, Schulze RJ, Martin R, Lycklama ANJA, Lee SC (2016) Membrane protein insertion and assembly by the bacterial holo-translocon SecYEG-SecDF-YajC-YidC. Biochem J 473:3341–3354. https://doi.org/10.1042/bcj20160545

Kumar M, Chatterji D (2008) Cyclic di-GMP: a second messenger required for long-term survival, but not for biofilm formation, in mycobacterium smegmatis. Microbiol (reading) 154:2942–2955. https://doi.org/10.1099/mic.0.2008/017806-0

Kutschera A, Schombel U, Schwudke D, Ranf S, Gisch N (2021) Analysis of the structure and biosynthesis of the lipopolysaccharide core oligosaccharide of *Pseudomonas syringae* pv. tomato DC3000. Int J Mol Sci. 22:3250. https://doi.org/10.3390/ijms22063250

Lee SW, Glickmann E, Cooksey DA (2001) Chromosomal locus for cadmium resistance in Pseudomonas putida consisting of a cadmium-transporting ATPase and a MerR family response regulator. Appl Environ Microbiol 67:1437–1444. https://doi.org/10.1128/aem.67.4.1437-1444.2001

Létoffé S, Chalabaev S, Dugay J, Stressmann F, Audrain B, Portais JC (2017) Biofilm microenvironment induces a widespread adaptive amino-acid fermentation pathway conferring strong fitness advantage in *Escherichia coli*. PLoS Genet 13:e1006800. https://doi.org/10.1371/journal.pgen.1006800

Li L, Meng H, Gu D, Li Y, Jia M (2019) Molecular mechanisms of *Vibrio parahaemolyticus* pathogenesis. Microbiol Res 222:43–51. https://doi.org/10.1016/j.micres.2019.03.003

McCool GJ, Cannon MC (2001) PhaC and PhaR are required for polyhydroxyalkanoic acid synthase activity in bacillus megaterium. J Bacteriol 183:4235–4243. https://doi.org/10.1128/jb.183.14.4235-4243.2001

Melo-López FN, Zermeño-Cervantes LA, Barraza A, Loera-Muro A, Cardona-Félix CS (2021) Biochemical characterization of LysVpKK5 endolysin from a marine vibrio phage. Protein Expr Purif 188:105971. https://doi.org/10.1016/j.pep.2021.105971

Miller KD, Pniewski K, Perry CE, Papp SB, Shaffer JD, Velasco-Silva JN (2021) Targeting ACSS2 with a transition-state mimetic inhibits triple-negative breast cancer growth. Cancer Res 81:1252–1264. https://doi.org/10.1158/0008-5472.Can-20-1847

Minárik P, Tomásková N, Kollárová M, Antalík M (2002) Malate dehydrogenases-structure and function. Gen Physiol Biophys 21:257–265

Moosavi B, Berry EA, Zhu XL, Yang WC, Yang GF (2019) The assembly of succinate dehydrogenase: a key enzyme in bioenergetics. Cell Mo Life Sci 76:4023–4042. https://doi.org/10.1007/s00018-019-03200-7

Murray KA, Escobar LE, Lowe R, Rocklöv J, Semenza JC, Watts N (2020) Tracking infectious diseases in a warming world. BMJ 371:m3086. https://doi.org/10.1136/bmj.m3086

Obbard JP, Sauerbeck D, Jones KC (1994) Dehydrogenase activity of the microbial biomass in soils from a field experiment amended with heavy metal contaminated sewage sludges. Sci Total Environ 142:157–162. https://doi.org/10.1016/0048-9697(94)90323-9

Oschlies A, Brandt P, Stramma L, Schmidtko S (2018) Drivers and mechanisms of ocean deoxygenation. Nat Geosci 11:467–473. https://doi.org/10.1038/s41561-018-0152-2

Pal C, Bengtsson-Palme J, Rensing C, Kristiansson E, Larsson DG (2014) BacMet: antibacterial biocide and metal resistance genes database. Nucleic Acids Res 42:D737–743. https://doi.org/10.1093/nar/gkt1252

Pazhani GP, Chowdhury G, Ramamurthy T (2021) Adaptations of *Vibrio parahaemolyticus* to stress during environmental survival, host colonization,

and infection. Front Microbiol 12:737299. https://doi.org/10.3389/fmicb.2021.737299

Pohl A, Ridgwell A, Stockey RG, Thomazo C, Keane A, Vennin E (2022) Continental configuration controls ocean oxygenation during the Phanerozoic. Nature 608:523–527. https://doi.org/10.1038/s41586-022-05018-z

Ramamurthy T, Nandy RK, Mukhopadhyay AK, Dutta S, Mutreja A, Okamoto K (2020) Virulence regulation and innate host response in the pathogenicity of *Vibrio cholerae*. Front Cell Infect Microbiol 10:572096. https://doi.org/10.3389/fcimb.2020.572096

Raval IH, Labala RK, Raval KH, Chatterjee S, Haldar S (2021) Characterization of VopJ by modelling, docking and molecular dynamics simulation with reference to its role in infection of enteropathogen *Vibrio parahaemolyticus*. J Biomol Struct Dyn 39:1572–1578. https://doi.org/10.1080/07391102.2020.1734486

Reaney SH, Smith DR (2005) Manganese oxidation state mediates toxicity in PC12 cells. Toxicol Appl Pharmacol 205:271–281. https://doi.org/10.1016/j.taap.2004.10.013

Rosario MM, Fredrick KL, Ordal GW, Helmann JD (1994) Chemotaxis in bacillus subtilis requires either of two functionally redundant CheW homologs. J Bacteriol 176:2736–2739. https://doi.org/10.1128/jb.176.9.2736-2739.1994

Rubio Gomez MA, Ibba M (2020) Aminoacyl-tRNA Synthetases Rna 26:910–936. https://doi.org/10.1261/rna.071720.119

Sędzielewska K, Böer E, Bellebna C, Wartmann T, Bode R, Melzer M (2012) Role of the AFRD1-encoded fumarate reductase in hypoxia and osmotolerance in Arxula adeninivorans. FEMS Yeast Resn 12:924–937. https://doi.org/10.1111/j.1567-1364.2012.00842.x

Spidlova P, Stojkova P, Dankova V, Senitkova I, Santic M, Pinkas D (2018) Francisella tularensis D-Ala carboxypeptidase DacD is involved in intracellular replication and it is necessary for bacterial cell wall integrity. Front Cell Infect Microbiol 8:111. https://doi.org/10.3389/fcimb.2018.00111

Stamatakis A (2014) RAxML version 8: A tool for phylogenetic analysis and post-analysis of large phylogenies. Bioinformatics 30:1312–1313. https://doi.org/10.1093/bioinformatics/btu033

Su C, Chen L (2020) Virulence, resistance, and genetic diversity of *Vibrio parahaemolyticus* recovered from commonly consumed aquatic products in Shanghai. China Mar Pollut Bull 160:111554. https://doi.org/10.1016/j.marpolbul.2020.111554

Sun X, Liu T, Peng X, Chen L (2014) Insights into *Vibrio parahaemolyticus* CHN25 response to artificial gastric fluid stress by transcriptomic analysis. Int J Mol Sc 15:22539–22562. https://doi.org/10.3390/ijms151222539

Sun H, Zhu C, Fu X, Khattak S, Wang J, Liu Z (2022) Effects of intestinal microbiota on physiological metabolism and pathogenicity of Vibrio. Front Microbiol 13:947767. https://doi.org/10.3389/fmicb.2022.947767

Tempel S, Bedo J, Talla E (2022) From a large-scale genomic analysis of insertion sequences to insights into their regulatory roles in prokaryotes. BMC Genomics 23:451. https://doi.org/10.1186/s12864-022-08678-3

Thi MTT, Wibowo D, Rehm BHA (2020) *Pseudomonas* aeruginosa biofilms. Int J Mol Sci 21:8671. https://doi.org/10.3390/ijms21228671

Thurm C, Schraven B, Kahlfuss S (2021) ABC Transporters in T cell-mediated physiological and pathological immune responses. Int J Mol Sci 22:9186. https://doi.org/10.3390/ijms22179186

Tian D, Wang Y, Xing J, Sun Q, Song J, Li X (2020) Nitrogen loss process in hypoxic seawater based on the culture experiment. Mar Pollut Bull 152:110912. https://doi.org/10.1016/j.marpolbul.2020.110912

Tierney AR, Rather PN (2019) Roles of two-component regulatory systems in antibiotic resistance. Future Microbiol 14:533–552. https://doi.org/10.2217/fmb-2019-0002

Tong S, Bambrick H, Beggs PJ, Chen L, Hu Y, Ma W (2022) Current and future threats to human health in the Anthropocene. Environ Int 158:106892. https://doi.org/10.1016/j.envint.2021.106892

Turi Z, Lacey M, Mistrik M, Moudry P (2019) Impaired ribosome biogenesis: mechanisms and relevance to cancer and aging. Aging (Albany NY) 11:2512–2540. https://doi.org/10.18632/aging.101922

Tuttle MJ, May FS, Basso JTR, Gann ER, Xu J, Buchan A (2022) Plasmid-mediated stabilization of prophages. Msphere 7:e0093021. https://doi.org/10.1128/msphere.00930-21

Uchida Y, Yamamoto Y, Sakisaka T (2021) Trans-2-enoyl-CoA reductase limits Ca^{2+} accumulation in the endoplasmic reticulum by inhibiting the Ca^{2+} pump $SERCA_2b$. J Biol Chem 296:100310. https://doi.org/10.1016/j.jbc.2021.100310

Xu *et al. Annals of Microbiology*   (2024) 74:20

Page 23 of 23

Vu TTT, Hoang TTH, Fleischmann S, Pham HN, Lai TLH, Cam TTH (2022) Quantification and antimicrobial resistance of *Vibrio parahaemolyticus* in retail seafood in hanoi. Vietnam J Food Prot 85:786–791. https://doi.org/10.4315/jfp-21-444

Wahl A, Battesti A, Ansaldi M (2019) Prophages in salmonella enterica: a driving force in reshaping the genome and physiology of their bacterial host? Mol Microbiol 111:303–316. https://doi.org/10.1111/mmi.14167

Wamp S, Rutter ZJ, Rismondo J, Jennings CE, Möller L, Lewis RJ (2020) PrkA controls peptidoglycan biosynthesis through the essential phosphorylation of ReoM. Elife 9:e56048. https://doi.org/10.7554/eLife.56048

Wang LP, Zhou SX, Wang X, Lu QB, Shi LS, Ren X (2021) Etiological, epidemiological, and clinical features of acute diarrhea in China. Nat Commun 12:2464. https://doi.org/10.1038/s41467-021-22551-z

Wilson DF (2017) Oxidative phosphorylation: regulation and role in cellular and tissue metabolism. J Physiol 595:7023–7038. https://doi.org/10.1113/jp273839

Xu D, Peng X, Xie L, Chen L (2022a) Survival and genome diversity of *Vibrio parahaemolyticus* isolated from edible aquatic animals. Diversity 14:350. https://doi.org/10.3390/d14050350

Xu Y, Yang L, Wang Y, Zhu Z, Yan J, Qin S, Chen L (2022b) Prophage-encoded gene *VpaChn25_0734* amplifies ecological persistence of *Vibrio parahaemolyticus* CHN25. Curr Genet 68:267–287. https://doi.org/10.1007/s00294-022-01229-z

Yang N, Liu M, Luo X, Pan J (2015) Draft genome sequence of strain ATCC17802T, the type strain of *Vibrio parahaemolyticus*. Mar Genomics 24:203–205. https://doi.org/10.1016/j.margen.2015.05.010

Yang L, Wang Y, Yu P, Ren S, Zhu Z, Jin Y, Yan J, Peng X, Chen L (2020) Prophage-related gene *VpaChn25_0724* contributes to cell membrane integrity and growth of *Vibrio parahaemolyticus* CHN25. Front Cell Infect Microbiol 10:595709. https://doi.org/10.3389/fcimb.2020.595709

Yao W, Yang L, Shao Z, Xie L, Chen L (2020) Identification of salt tolerance-related genes of *Lactobacillus plantarum* D31 and T9 strains by genomic analysis. Ann Microbiol 70:10. https://doi.org/10.1186/s13213-020-01551-2

Yildiz FH, Visick KL (2009) *Vibrio* biofilms: so much the same yet so different. Trends Microbiol 17:109–118. https://doi.org/10.1016/j.tim.2008.12.004

Yu P, Yang L, Wang J, Su C, Qin S, Zeng C, Chen L (2022) Genomic and transcriptomic analysis reveal multiple strategies for the cadmium tolerance in *Vibrio parahaemolyticus* N10–18 isolated from aquatic animal ostrea gigas thunberg. Foods 11:3777. https://doi.org/10.3390/foods11233777

Zaayman M, Wheatley RM (2022) Fitness costs of CRISPR-Cas systems in bacteria. Microbiology (reading) 168:7. https://doi.org/10.1099/mic.0.001209

Zhai Y, Meng X, Li L, Liu Y, Xu K, Zhao C (2021) Rapid detection of *Vibrio parahaemolyticus* using magnetic nanobead-based immunoseparation and quantum dot-based immunofluorescence. RSC Adv 11:38638–38647. https://doi.org/10.1039/d1ra07580b

Zhang K, Chen D, Ma K, Wu X, Hao H, Jiang S (2018) NAD(P)H: Quinone Oxidoreductase 1 (NQO1) as a therapeutic and diagnostic target in cancer. J Med Chem 61:6983–7003. https://doi.org/10.1021/acs.jmedchem.8b00124

Zhu Z, Yang L, Yu P, Wang Y, Peng X, Chen L (2020) Comparative proteomics and secretomics revealed virulence and antibiotic resistance-associated factors in *Vibrio parahaemolyticus* recovered from commonly consumed aquatic products. Front Microbiol 11:1453. https://doi.org/10.3389/fmicb.2020.01453

Publisher's Note